PAPER

JET and COMPASS asymmetrical disruptions

To cite this article: S.N. Gerasimov *et al* 2015 *Nucl. Fusion* **55** 113006

IOP Publishing | International Atomic Energy Agency Nuclear Fusion

Nucl. Fusion **55** (2015) 113006 (18pp) doi:10.1088/0029-5515/55/11/113006

JET and COMPASS asymmetrical disruptions

S.N. Gerasimov[1], P. Abreu[2], M. Baruzzo[3], V. Drozdov[1], A. Dvornova[4], J. Havlicek[5,6], T.C. Hender[1], O. Hronova[5], U. Kruezi[1], X. Li[7], T. Markovič[5,6], R. Pánek[5], G. Rubinacci[8], M. Tsalas[9], S. Ventre[10], F. Villone[10], L.E. Zakharov[11] and JET Contributors[a]

EUROfusion Consortium, JET, Culham Science Centre, Abingdon, OX14 3DB, UK
[1] CCFE, Culham Science Centre, Abingdon, OX14 3DB, UK
[2] Instituto de Plasmas e Fusão Nuclear, Instituto Superior Técnico, Universidade de Lisboa, Portugal
[3] ENEA, Frascati, Italy
[4] NRNU MEPhI, 115409, Kashirskoe sh. 31, Moscow, Russia
[5] Institute of Plasma Physics AS CR, Za Slovankou 3, 182 21 Praha 8, Czech Republic
[6] Charles University in Prague, Faculty of Mathematics and Physics, Ke Karlovu 3, 121 16, Prague 2, Czech Republic
[7] Institute of Computational Mathematics and Scientific/Engineering Computing, Academy of Mathematics and Systems Science, Chinese Academy of Sciences, PO Box 2719, Beijing 100190, People's Republic of China
[8] ENEA/CREATE, DIETI, Università di Napoli Federico II, Italy
[9] FOM Inst. DIFFER, Nieuwegein, Netherlands
[10] ENEA/CREATE, DIEI, Università di Cassino, Italy
[11] PPPL, Princeton University, Princeton, NJ 08543, USA

E-mail: Sergei.Gerasimov@ccfe.ac.uk

Received 30 April 2015, revised 1 July 2015
Accepted for publication 16 July 2015
Published 8 September 2015

Abstract

Asymmetrical disruptions may occur during ITER operation and they may be accompanied by large sideways forces and rotation of the asymmetry. This is of particular concern because resonance of the rotating asymmetry with the natural frequencies of the vacuum vessel (and other in-vessel components) could lead to large dynamic amplification of the forces. A significant fraction of non-mitigated JET disruptions have toroidally asymmetric currents that flow partially inside the plasma and partially inside the surrounding vacuum vessel ('wall'). The toroidal asymmetries (otherwise known as the appearance of 3D structures) are clearly visible in the plasma current (I_p) and the first plasma current moments. For the first time we present here the asymmetries in toroidal flux measured by the diamagnetic loops and also propose a physical interpretation. The presented data covers the period of JET operation with a C-wall (JET-C from 2005 until late 2009) and with an ITER-like wall (JET-ILW from 2011 until late 2014), during which pick-up coil and saddle loop data at four toroidally orthogonal locations were routinely recorded. The observed rotations of the I_p asymmetries are in the range from -5 turns to $+10$ turns (a negative value is counted to the negative plasma current). Initial observations on COMPASS of asymmetric disruptions are presented, which are in line with JET data. The whole of the JET-ILW disruption database and the limited number of COMPASS disruptions examined confirm that the development of the toroidal asymmetry precedes the drop to unity of q95. It is shown that massive gas injection (MGI), which is routinely used to mitigate disruptions, significantly reduces the I_p asymmetries in JET. However, MGI produces fast plasma current quench and consequently high vessel eddy currents, which expose the machine to additional stresses. The effect of the large gas quantity used during the injection is of particular concern as well.

[a] See the appendix of [53].

Keywords: tokamak, asymmetrical disruption, JET, COMPASS

(Some figures may appear in colour only in the online journal)

1. Introduction

Asymmetrical disruptions [1] may occur during ITER operations [2]. It is possible that they may be accompanied by large sideways forces and by toroidal rotation of the asymmetry. The toroidal rotation of the sideways force is of particular concern because resonance with the natural frequencies of the vacuum vessel (and other in-vessel components) could lead to large dynamic amplification of the forces [3, 4]. As a result of disruptions, the JET vacuum vessel can undergo a complex, damped oscillation with a peak displacement in the order of a few mm [5, 6]. The observation of 3D effects (or in other words toroidal and poloidal asymmetries) during the plasma current (I_p) quench has been described in many tokamaks using various diagnostics, e.g. JET [7–15], JT60-U [16], Alcator C-Mod [17], DIII-D [18], ASDEX-U [19] and NSTX [20, 21]. The theory, modelling and interpretation of the 3D effects during the I_p current quench (CQ) can be found in references including [1, 8, 14, 22–32].

JET is the only tokamak which has published data of plasma current moments at four orthogonal toroidal locations [1, 9–15]. COMPASS has the capability to measure I_p at three toroidal locations (two of which are opposite) [15].

A significant fraction of all JET non-mitigated disruptions have toroidally asymmetric currents that flow partially inside the plasma and partially inside the surrounding vacuum vessel ('wall'). The toroidal asymmetries are clearly visible in the I_p, the first plasma current moments and in-vessel poloidal voltages, i.e. toroidal magnetic flux derivatives. The presented data covers the period of JET operation with a C-wall (JET-C from 2005 until late 2009) and with an ITER-like wall (JET-ILW [33–36] from 2011 until late 2014), during which pick-up coil and saddle loop data at four toroidally orthogonal locations were routinely recorded. The I_p asymmetries in JET usually rotate in either toroidal direction, showing substantial variation in magnitude and frequency. Initial observations on COMPASS of asymmetric disruptions are presented, which are in line with JET data.

The whole of the JET-ILW disruption database, and the limited number of COMPASS disruptions examined, indicate that axisymmetric and asymmetrical disruptions have dissimilar time behaviour of the edge safety factor, namely the development of the toroidal asymmetry precedes the drop of q95.

In addition to toroidal asymmetry of the plasma current, we report here the asymmetry in the poloidal voltage (diamagnetic signal derivative) and its physical interpretation.

Massive gas injection (MGI) is routinely used to mitigate disruptions in JET, if $I_p > 2$ MA or the total plasma energy (poloidal magnetic + kinetic) is above 5 MJ [37–40]. It is shown here that MGI can significantly reduce the I_p asymmetries during the plasma CQ and sideways forces. However, the MGI leads to a strong uncontrollable decrease of CQ duration, which in turn increases the induced vessel currents and axisymmetric forces. The effect of the large gas quantity used during the injection is of particular concern as well.

This paper extends the results presented in [14, 15]. Diagnostics used in JET and COMPASS are described in section 2. The composition of the plasma current asymmetry database is given in section 3. Sideways force impulses and JET vessel displacements, which were extracted over a 9 year period of JET operation, are outlined in section 4. JET and COMPASS I_p asymmetry data are presented in section 5. The rotation of the plasma current asymmetries is given in section 6. The edge safety factor at disruption is sketched in section 7. Asymmetry in the toroidal magnetic flux and its physical interpretation can be found in section 8. Experimental and computational results on axisymmetric eddy currents and MGI issues are discussed in section 9. Outstanding issues, which are the subject of future investigations, are described in section 10. The results of the disruption analyses in terms of various toroidal asymmetries are summarised in section 11.

2. JET and COMPASS magnetic diagnostics

JET magnetic diagnostic data from 18 tangential to vessel pick-up coils and 14 normal saddles [14] at four toroidally orthogonal locations has been routinely recorded from 2005 onwards (see figures 1 and 2). Two poloidal in-vessel loop voltages at toroidally opposite locations (see figures 1 and 3) were used to evaluate toroidal (paramagnetic) flux asymmetry during the CQ.

The ex-vessel Rogowski coil, in-vessel pick-up coils and four in-vessel full toroidal flux loops were used to calculate the total axisymmetric toroidal eddy current in the conductive structures of the vessel, restraining ring, divertor support structure and poloidal field (PF) coil cases; see figure 4.

The JET Rogowski coil measures the plasma current (I_p), total divertor PF coil current (I_D) and the eddy current induced in the conductive structures (I_{pst}): vessel (I_{ves}), restraining ring (I_{RR}), divertor support structure and PF coil cases (I_{MARK}):

$$I_{rog} = I_p + I_D + I_{pst}, \text{ where } I_{pst} = I_{ves} + I_{RR} + I_{MARK}. \quad (1)$$

The plasma current is

$$I_p = I_{pla}^{IDC} - I_D - I_{RR} - I_{MARK}, \quad (2)$$

where I_{pla}^{IDC} is the uncorrected plasma current calculated using 18 internal discrete coils [14]. Hence the total induced toroidal passive structure current is defined as

$$I_{pst} = I_{rog} - I_p - I_D = I_{rog} - I_{pla}^{IDC} + I_{RR} + I_{MARK}. \quad (3)$$

The restraining ring current, divertor support structure and PF case current are calculated from the relevant voltage measurements:

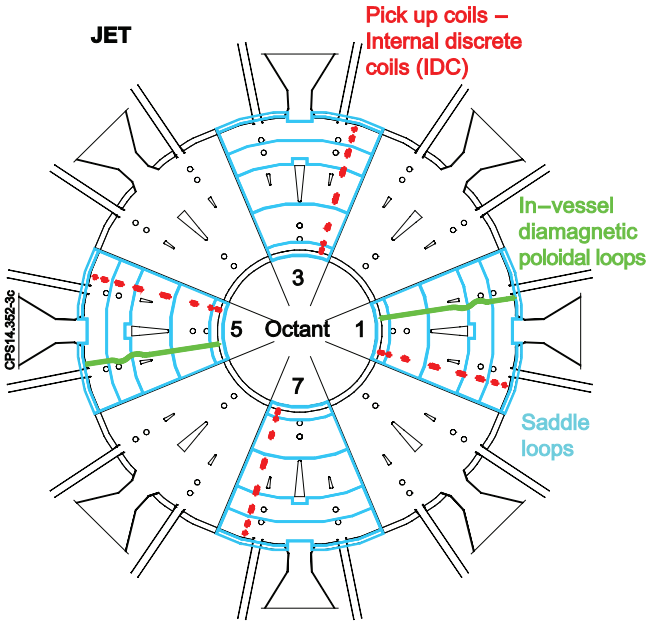

Figure 1. Plan view of JET magnetic diagnostics.

$$I_{\mathrm{RR}} = (\mathrm{VLRRU} + \mathrm{VLRRL})/R_{\mathrm{RR}},\ R_{\mathrm{RR}} = 1.4\,m\mathrm{Ohm}, \quad (4)$$

$$I_{\mathrm{MARK}} = \tfrac{1}{2}(\mathrm{VLD\,2} + \mathrm{VLD\,3})/R_{\mathrm{MARK}},$$

$$R_{\mathrm{MARK}} = 0.739\ m\mathrm{Ohm}, \quad (5)$$

where VLRRU, VLRRL, VLD2 and VLD3 are toroidal voltages from the relevant full flux loops (see figure 4).

The horizontal (radial) JET vessel displacements are measured at vertical ports of each vessel octant with respect to the mechanical structure [41]; see figure 2. JET magnetic data are recorded at a 5 kHz sampling rate and vessel force and displacement data are recorded at a 2.5 kHz sampling rate around a disruption, which is sufficient taking into account that the duration of CQ $\geqslant$ ~10 ms.

At present, COMPASS I_{p} in-vessel magnetic diagnostics are available at three toroidal locations, two of which are opposite and the third is shifted in respect to the other by 45° [42, 43]; see figure 5. Therefore the relevant plasma currents are

1. I_{p1} measured by an internal Rogowski coil near toroidal field coil (TFC) #1;
2. I_{p9} calculated from 16 tangential pick-up (internal partial Rogowski) coils near TFC #9;
3. I_{p15} calculated from 24 tangential pick-up (Mirnov) coils near TFC #15.

Hence the difference in the I_{p} at opposite locations is defined as $\Delta I_{\mathrm{p91}} = I_{\mathrm{p9}} - I_{\mathrm{p1}}$. The COMPASS data is recorded at a 2 MHz sampling rate.

3. JET and COMPASS database

The presented JET four-octant data (with pre-disruptive plasma current $I_{\mathrm{p}}^{\mathrm{dis}} \geqslant 1$ MA [14]) covers 1990 disruptions from 3/11/2005 (#64326) up to 9/10/2014 (#87944) including both JET-C (950 disruptions) and JET-ILW (1040 disruptions).

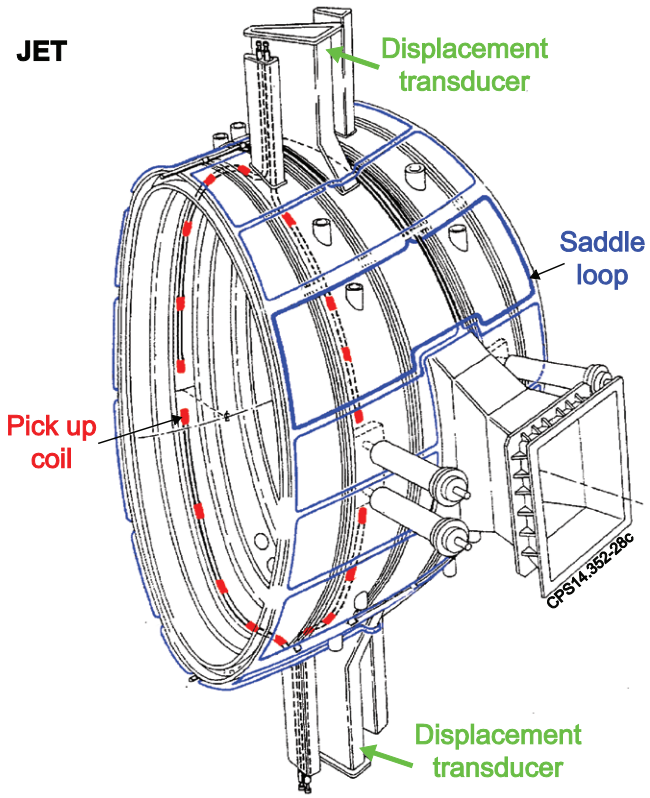

Figure 2. JET pick-up coils, saddle loops and vessel radial displacement transducers.

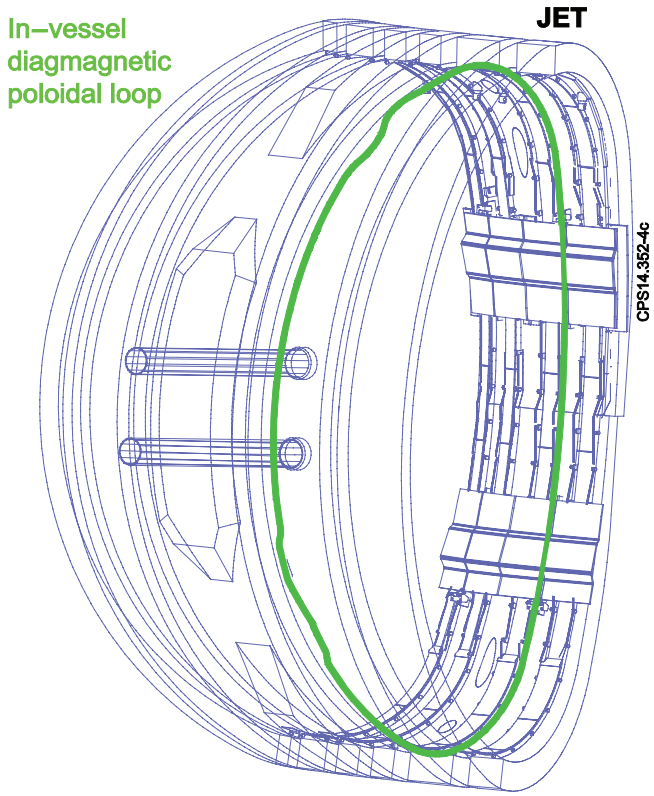

Figure 3. Two JET opposite vessel octants equipped with in-vessel (diamagnetic) poloidal loops.

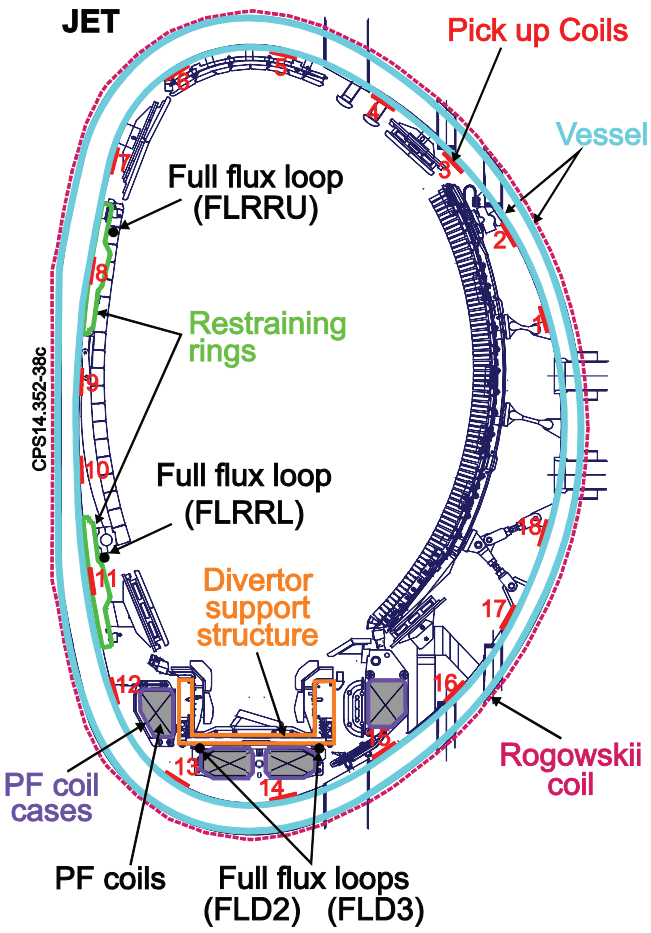

Figure 4. JET diagnostics (ex-vessel Rogowski coil, in-vessel pick-up coils and four in-vessel full toroidal flux loops) used to calculate the total toroidal eddy current in a conductive structure: vessel, restraining rings, divertor support structure and PF coil cases.

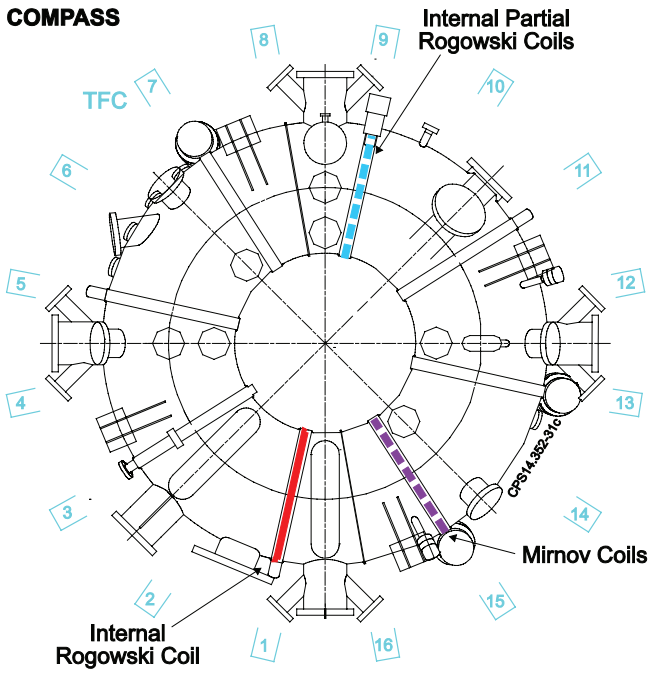

Figure 5. Plan view of COMPASS I_p diagnostics.

The section below describes the mathematical background, which was used in calculating the key parameters of the I_p toroidal asymmetries, or in other words, 3D structures. For modelling the toroidal angle dependency of the plasma current, a Fourier series was used.

The toroidal variation of the measured plasma current is approximated by a finite Fourier sum, which is also called a trigonometric polynomial of degree n:

$$I_p^n(\varphi) = X_o + \sum_{k=1}^{n}[X_k \cos(k\varphi) + Y_k \sin(k\varphi)], \tag{6}$$

where φ is the toroidal angle, k is the toroidal harmonic number, and X_o (representing the toroidally averaged plasma current), X_k and Y_k are Fourier coefficients. In general, if the number of measurements, m, is sufficient ($m \geqslant 2n+1$), these Fourier coefficients can be found using the least squares method by solving the minimisation problem:

$$\min \sum_{j}^{m}[\delta I(\varphi_j)]^2,\ 1 \leqslant j \leqslant m, \tag{7}$$

where a residual is defined as $\delta I(\varphi_j) = I_P^n(\varphi_j) - I_p(\varphi_j)$, $I_p(\varphi_j)$ is measured plasma current and $I_p^n(\varphi_j)$ is the value predicted by the model at toroidal angle φ_j.

Taking into account that the number of measurements for JET $m = 4$ and for COMPASS $m = 3$, we approximate the 3D plasma current by a trigonometric polynomial $n = 1$ for both machines:

$$I_p(\varphi) = X_o + X_1 \cos(\varphi) + Y_1 \sin(\varphi). \tag{8}$$

Hence the minimisation problem (7) with condition (8) unambiguously gives three equations for three Fourier coefficients:

$$\begin{aligned} \sum_{j=1}^{m} \delta I(\varphi_j) &= 0 \\ \sum_{j=1}^{m} \delta I(\varphi_j) \cdot \cos(\varphi_j) &= 0 \\ \sum_{j=1}^{m} \delta I(\varphi_j) \cdot \sin(\varphi_j) &= 0. \end{aligned} \tag{9}$$

For JET with $m = 4$ measurements, the residual in (7) becomes:

$$\begin{aligned} \delta I(\varphi_1) &= -I_p(\varphi_1) + X_o + X_1, \quad \varphi_1 = 0, \quad I_p(\varphi_1) \equiv I_{p1} \\ \delta I(\varphi_2) &= -I_p(\varphi_2) + X_o + Y_1, \quad \varphi_2 = \pi/2, \quad I_p(\varphi_2) \equiv I_{p3} \\ \delta I(\varphi_3) &= -I_p(\varphi_3) + X_o - X_1, \quad \varphi_3 = \pi, \quad I_p(\varphi_3) \equiv I_{p5} \\ \delta I(\varphi_4) &= -I_p(\varphi_4) + X_o - Y_1, \quad \varphi_4 = 3\pi/2 \quad I_p(\varphi_4) \equiv I_{p7}, \end{aligned} \tag{10}$$

where I_{p1} = octant #1 plasma current measurement, etc.

Then the solution of (9) is:

$$\begin{aligned} X_o &= (I_{p1} + I_{p3} + I_{p5} + I_{p7})/4 \\ X_1 &= (I_{p1} - I_{p5})/2 \\ Y_1 &= (I_{p3} - I_{p7})/2. \end{aligned} \tag{11}$$

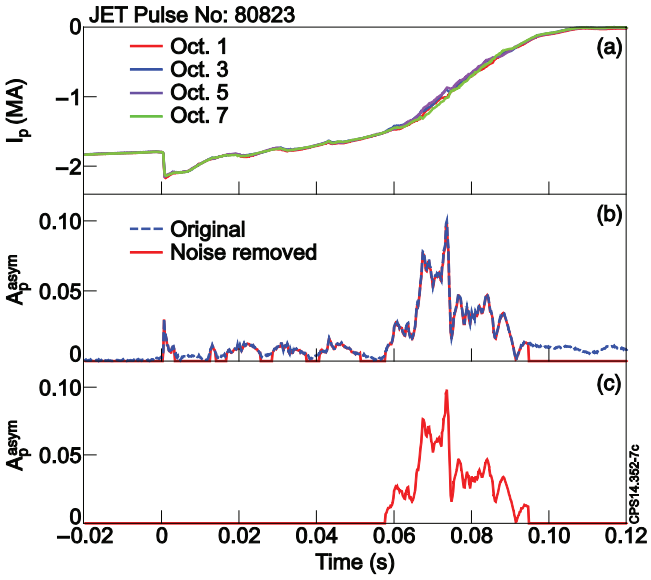

Figure 6. The composition of the trimmed waveforms: (*a*) plasma currents, (*b*) normalised I_p asymmetries, (*c*) asymmetry main window. The time axis is normalised to T_{dis}; see detailed explanation of T_{dis} in [14].

The absolute $I_p^{asym} = 2\sqrt{X_1^2 + Y_1^2} \equiv \sqrt{(I_{p7} - I_{p3})^2 + (I_{p5} - I_{p1})^2}$ and normalised $A_p^{asym} = I_p^{asym}/\left|I_p^{dis}\right|$ quantities are used to characterise the magnitude of I_p asymmetries. Unlike C-wall disruptions in JET, the IL-wall disruptions can undertake several I_p asymmetry bursts during the CQ. To take into account the specific properties of the IL-wall, the conditions of the database composition were modified in comparison with [14]. Namely to avoid noise contributing to the results, I_p^{asym} (and A_p^{asym}) is only calculated for times when the start and end time window satisfied the following conditions: $A_p^{asym} > 0.5\%$ and $|I_p| > 0.1\left|I_p^{dis}\right|$ for the first and last 1 ms in order to disregard short-lived spikes. The A_p^{asym} values that do not satisfy the criteria are treated as noise and forced to zero. The above-defined time window was applied to all time-dependent quantities which have been used for analysis. Additionally, a new constraint was introduced; namely if $I_p^{asym} \leqslant 10$ kA (10 kA is the error in JET I_p measurements) for 2 ms inside the 'asymmetry window' then waveforms are forced to zero during this interval, resulting in the concept of a 'main asymmetry time window' (the largest $A = \int A_p^{asym} dt$ for which $I_p^{asym} \neq 0$). Using the main asymmetry time window, the effects of noise in the analysis have been reduced. Figure 6 explains the composition of the waveforms that have been used for the presented JET analysis.

The COMPASS disruption database is currently under development and some data are presented below. The presented COMPASS asymmetrical disruption data cover 78 C-wall shots from 12/11/2013 (#6033) up to 27/11/2014 (#8788).

Since COMPASS has $m = 3$ toroidal I_p measurements, the residual in (7) becomes:

$$\begin{aligned}
\delta I(\varphi_1) &= -I_p(\varphi_1) + X_o + X_1, && \varphi_1 = 0, && I_p(\varphi_1) \equiv I_{p1} \\
\delta I(\varphi_2) &= -I_p(\varphi_2) + X_o + X_1/\sqrt{2} + Y_1/\sqrt{2}, && \varphi_2 = \pi/4, && I_p(\varphi_2) \equiv I_{p15} \\
\delta I(\varphi_3) &= -I_p(\varphi_3) + X_o - X_1, && \varphi_3 = \pi, && I_p(\varphi_3) \equiv I_{p9}.
\end{aligned} \tag{12}$$

Then the solution of (9) is:

$$\begin{aligned}
X_o &= (I_{p1} + I_{p9})/2 \\
X_1 &= (I_{p1} - I_{p9})/2 \\
Y_1 &= \sqrt{2}\, I_{p15} - \frac{\sqrt{2}+1}{2} I_{p1} - \frac{\sqrt{2}-1}{2} I_{p9}.
\end{aligned} \tag{13}$$

COMPASS and JET use identical quantities to characterise the magnitude of I_p asymmetries, specifically $I_p^{asym} = 2\sqrt{X_1^2 + Y_1^2}$, $A_p^{asym} = I_p^{asym}/\left|I_p^{dis}\right|$ and $A = \int A_p^{asym} dt$ [14]. The A_p^{asym} can be estimated using only two opposite I_p measurements under an additional assumption, specifically only one harmonic, $Y_1 = 0$, then I_p^{asym} is reduced to $2\sqrt{X_1^2}$.

The data processing for COMPASS is similar to that of JET, and is comprised of the following steps:

1. ± 0.025 ms rectangular smoothing of the measured I_p to eliminate the noise contribution (JET uses ± 0.2 ms triangular smoothing on the final stage of processing to get peak quantities);
2. Trimming waveforms from left- and right-hand side where $A_p^{asym} > 2.0\%$ ($A_p^{asym} > 0.5\%$ for JET) or $|I_p| > 0.1\left|I_p^{dis}\right|$ conditions are not met;
3. A 'main asymmetry time window' was used; namely if $A_p^{asym} < 2.0\%$ for 0.1 ms ($I_p^{asym} < 10$ kA for 2 ms for JET) inside the 'asymmetry window' then waveforms are forced to zero during this interval.

There are some differences in the JET and COMPASS criteria reflecting the specific machine diagnostic properties.

An example of a COMPASS multi-turn I_p asymmetry rotational disruption is presented in figure 7. Box (b) shows A_p^{asym} calculated from three plasma currents (I_{p1}, I_{p9}, I_{p15}) – A_{3p}^{asym} and from only two (opposite) plasma currents (I_{p1}, I_{p9}) – A_{2p}^{asym}. The 3.5-turn uniform rotation window is shown in black in boxes (c) and (d). This specific time window (0.62 – 1.31 ms) was used to validate A_{3p}^{asym} in respect to A_{2p}^{asym}. The integral ratio over 0.62 – 1.31 ms is $A_3/A_2 \equiv \int A_{3p}^{asym} dt / \int A_{2p}^{asym} dt = 1.71$, whereas assuming a pure sine wave in time, the integral ratio must be $\pi/2$. This particular example proves that three and two I_p COMPASS measurements are self-consistent.

The $A_2/A_{3(2)}$ ratio over 77 (=78-1, since one shot has $A_2 = 0$) COMPASS asymmetrical disruptions, where the $A_{3(2)}$ integral is calculated over the A_2 time window, is shown in figure 8. The $2/\pi \leqslant A_2/A_{3(2)} \leqslant 1$ region contains the disruptions which have the toroidal phase of the I_p asymmetries dwelling mainly in quadrant #1 or #9, where the location of the centre of quadrant #1 is near TFC #1, etc. On the other hand, the $0 \leqslant A_2/A_{3(2)} \leqslant 2/\pi$ region contains the disruptions, which have I_p asymmetries dwelling mainly in quadrant #5 or #13. About 55% of the presented COMPASS disruptions (in terms of the toroidal phase of I_p asymmetry) were found in quadrant #5 or #13. Accordingly,

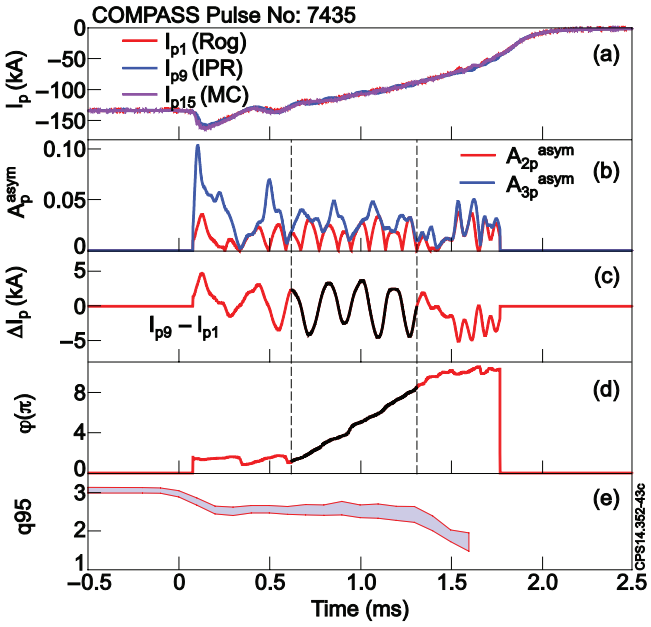

Figure 7. COMPASS multi-turn I_p asymmetry rotational disruption: (*a*) plasma currents, (*b*) amplitudes of the I_p asymmetries form I_{p1}, I_{p9}, I_{p15} (A_{3p}^{asym}) and I_{p1}, I_{p9} (A_{2p}^{asym}), (*c*) $\Delta I_p = I_{p9} - I_{p1}$ asymmetry, where 3.5-turn rotation is shown in black, (*d*) I_p asymmetry toroidal phase, (*e*) q95 edge safety factor. The time axis is normalised to T_{dis}.

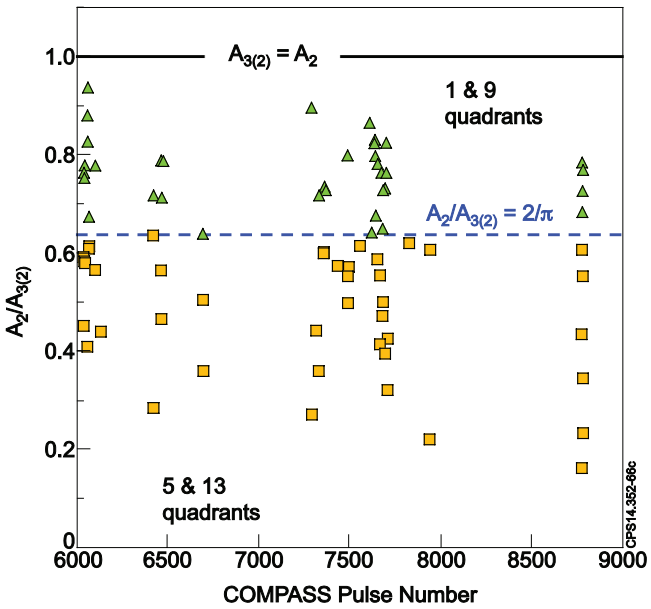

Figure 8. The $A_2/A_{3(2)}$ ratio allows definition of the dwelling of the I_p asymmetries: blue dashed line $A_2/A_{3(2)} = 2/\pi$ separates #1 and #9 quadrants from #5 and #13 quadrants.

45% of the disruptions were found in quadrant #1 or #9. We may conclude that for the present COMPASS three toroidal I_p measurements correctly provide an estimate of plasma current asymmetry in spite of the fact that diagnostic toroidal distribution is not optimal. However, as a precautionary measure, we are using different labels for shots dwelling mainly in quadrant #1 or #9 and in quadrant #5 or #13.

Apart from the I_p asymmetry data, sideways forces in JET can be evaluated using Noll's formula [1, 10, 14, 22],

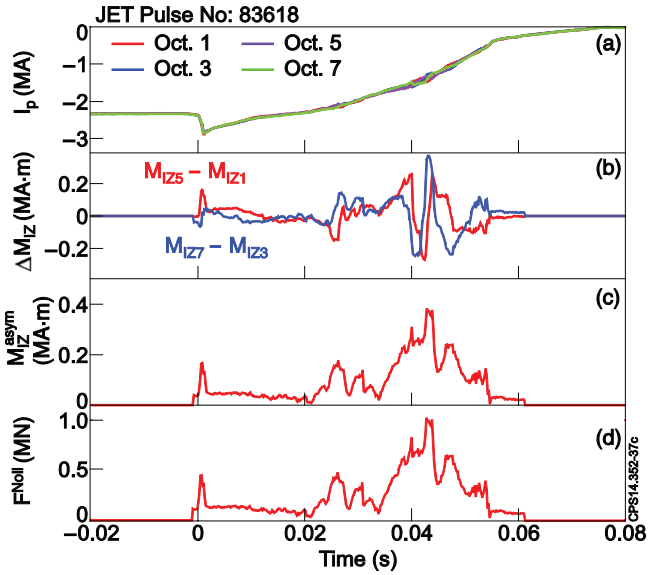

Figure 9. The sideways force impulses calculated from the measured M_{IZ} asymmetries: (*a*) plasma currents, (*b*) first vertical current moment asymmetries, (*c*) first vertical current moment asymmetry magnitude, (*d*) sideways force. The time axis is normalised to T_{dis}.

$F^{Noll} = \frac{\pi}{2} B_T M_{IZ}^{asym}$, where $M_{IZ}^{asym} = \sqrt{\Delta M_{IZx}^2 + \Delta M_{IZy}^2}$, $\Delta M_{IZy} \equiv \Delta M_{IZ73} = M_{IZ7} - M_{IZ3}$ and $\Delta M_{IZx} \equiv \Delta M_{IZ51} = M_{IZ5} - M_{IZ1}$ with M_{IZ1} = octant 1 first plasma current vertical moment, etc., see figure 9.

MGI (see figure 10) of a mixture (90% D_2 + 10% Ar) is routinely used to mitigate disruptions in JET, where the MGI fire criteria for the year 2014 were: $I_p > 2$ MA or total plasma energy (poloidal magnetic + kinetic) is above 5 MJ [37–40]. The MGI has a profound effect on 3D phenomena during the plasma CQ (see figure 11), hence the MGI shots are specifically labelled on the figures presented below.

4. Sideways force impulses and vessel displacements in JET

The sideways force impulse can be defined in two different ways. The first option is to calculate the impulse modulus, $\mathrm{Imp} = \int F^{Noll} dt$. The $F^{Noll} = \frac{\pi}{2} B_T \Delta M_{IZ}$ formula shown in [3] and was neatly derived in [41]. It is thought that the F^{Noll} formula gives the upper estimation for sideways force [25]. The plasma current moment expressions for JET can be found in [14]. The impulse modulus is a critical parameter in the case of a multi-turn rotational mode due to possible mechanical resonance of the machine components with the rotating force. It is a potentially serious issue for ITER, but not for JET, because the JET CQ duration is too short for multi-turn rotation within a vessel resonant period. The second option is to calculate the directional impulse, $\mathrm{Imp}_r = \sqrt{\mathrm{Imp}_x^2 + \mathrm{Imp}_y^2}$, where $\mathrm{Imp}_x = \int F_x^{Noll} dt = \frac{\pi}{2} B_T \int \Delta M_{IZy} dt$ and $\mathrm{Imp}_y = \int F_y^{Noll} dt = \frac{\pi}{2} B_T \int \Delta M_{IZx} dt$. The directional impulse is an essential parameter in the case of locked asymmetries, where the toroidal rotation slows and can remain stationary during a significant part

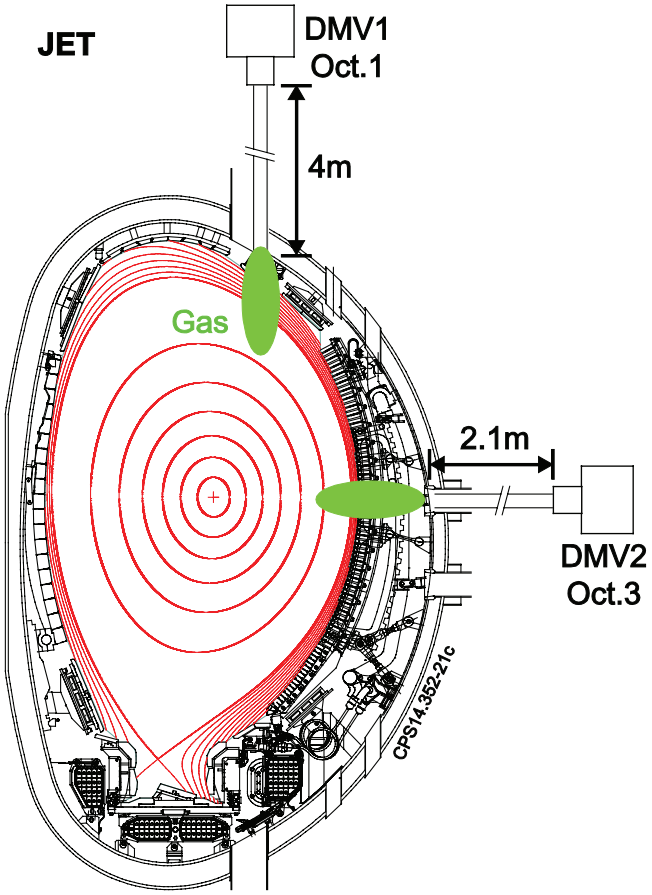

Figure 10. The location of the disruption mitigation valves (DMV) in JET.

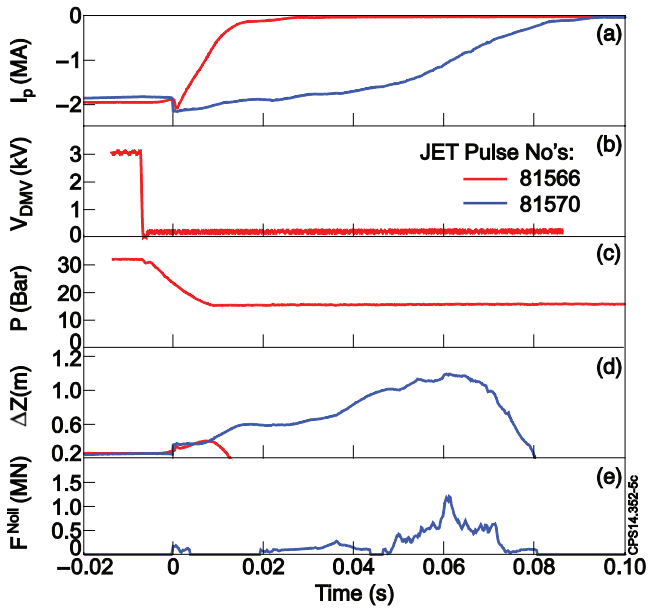

Figure 11. Comparing an MGI-mitigated disruption (red traces) and a non-mitigated disruption (blue traces) on disruption quantities: (*a*) plasma currents, (*b*) DMV1 voltage drop indicates the activation time, (*c*) DMV1 chamber pressure drop, (*d*) plasma current centroid vertical displacements, (*e*) sideways forces.

of the CQ. The directional impulse is always 'responsible' for sideways vessel displacement in JET for any rotational behaviour (see next page).

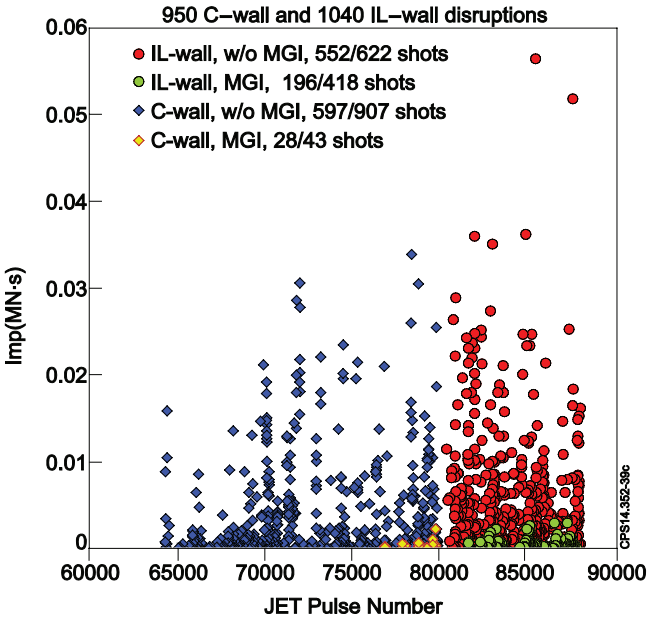

Figure 12. The impulse modulus for the JET four-octant database, where in the legend the first shot number indicates the number of asymmetrical disruptions and the second number is the total number of recorded disruptions.

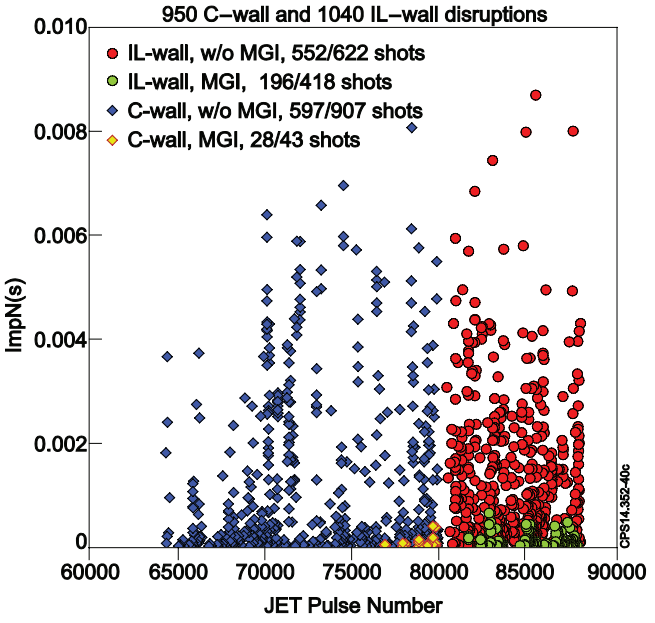

Figure 13. The normalised impulse moduli for the JET four-octant database.

The impulse moduli and the normalised impulse moduli (Imp$N$ = Imp/($B_T I_p a$), where the minor plasma radius, a, was taken as 1.00 m) for the JET four-octant database are presented in figures 12 and 13, respectively. It can be seen that MGI significantly reduces the sideways impulse moduli for both C- and IL-walls without exceptions.

As a result of asymmetrical disruptions, the JET vacuum vessel can undergo a complex, damped oscillation with a peak displacement in the order of a few mm with respect to the mechanical structure and the vessel can also experience violent mechanical forces in excess of a few MN [5, 6, 41]. The vessel supports can be represented as a damped spring-mass system

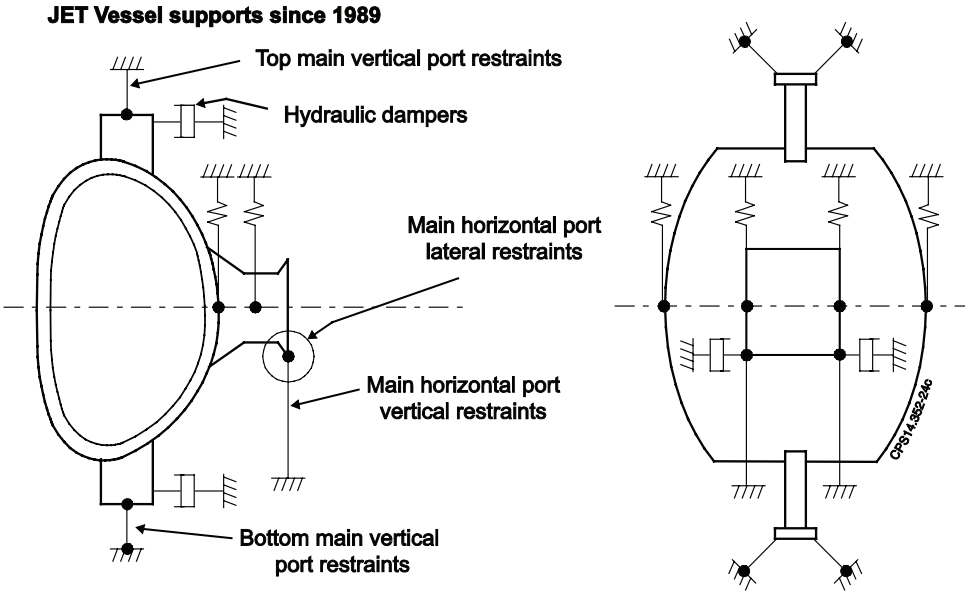

Figure 14. The current JET vessel supports; see detailed explanation in [41].

[41] with the mechanical resonance period of the vessel ~60–70 ms [41, 45], as shown in figure 14. An example of a complex, damped vessel oscillation due to an asymmetrical disruption is shown in figure 15. It can been seen that an asymmetrical vertical displacement event (VDE) has two phases, namely a first axisymmetric phase which is pure vertical displacement (m/n = 1/0 mode) and a second asymmetrical phase characterised by m/n = 1/1 dominated mode [14]. Hence, vertical force (F_z) and vessel roll arise at the same time (dashed line in figure 15) as exponential plasma vertical displacement. Sideways force (F^{Noll}) and vessel radial displacement start to grow in a second phase (dashed dotted line in figure 15).

The directional impulse Imp_r, which we believe is responsible for the radial vessel displacement, is compared with maximum vessel radial displacement over 1904 JET disruptions in figure 16. It indicates an approximately proportional relationship between magnetic and mechanical measurements, which is consistent with early limited JET data presented in [38, 41].

The distribution of the directional impulses in JET do not have a large degree of asymmetry over the toroidal angle; see figure 17. However, there is a preferred toroidal phase of the sideways force impulses which dwell mainly in quadrant #3.

The radial displacement mechanical measurements demonstrate a good correlation with magnetic diagnostic measurements in terms of magnitude and toroidal angle; see figure 18. Hence the estimation of the magnitude and direction of JET radial vessel displacement can be carried out with only the magnetic measurements.

In this paper we do not project the JET data to the larger machine. But we can confirm that the models described in [1, 25, 41] do not contradict the presented JET data. The simple scaling of JET sideways forces to ITER was made in [10], where it was noted that for the accurate calculation of the sideways forces a relevant wall model linked to kink mode evolution is needed. However, the scaling of the sideways force impulses (including mode duration and rotation) is the most difficult part of the forecast.

5. JET and COMPASS I_p asymmetry data

The magnitudes of the JET and COMPASS smoothed I_p asymmetry show a good agreement: the magnitude of I_p asymmetry is below ~20% of the pre-disruptive I_p for the whole range of the recorded disruptions in JET and COMPASS; see figure 19. However, instantaneous values of I_p asymmetry can potentially be affected by the noise pollution of the measured quantities and the chosen smoothing procedure.

Hence, a more reliable quantity [14], namely the integral $A = \int A_p^{\mathrm{asym}} \mathrm{d}t$ has been used to quantify the severity of I_p asymmetries. Figure 20 presents the normalised severity of I_p asymmetries as a function of the normalised CQ duration for the JET four-octant database and the present COMPASS database. The $\tau_{80\text{-}20}$ is the CQ time extrapolated from the time taken to quench from 80 to 20% of I_p^{dis}. The plasma cross-section area is not a reliable parameter during CQ, hence for comparison purposes $S = \pi a^2$ was calculated for circular plasma with the minor radius of the limiter, $a_{\mathrm{JET}} = 1.00\,m$ and $a_{\mathrm{COMPASS}} = 0.20\,m$. The maximum of the normalised integral of I_p asymmetry is located in the 2–15 ms m^{-2} domain of the normalised CQ duration. Although COMPASS data is in line with the large-scale JET database, the COMPASS outermost points are higher than the JET C-wall highest points by a factor of about 2. The extreme COMPASS disruption is shown in figure 21. Nevertheless, taking into account the relative size of COMPASS, JET and ITER, COMPASS and JET provide multi-machine identically treated disruption data that can be extrapolated to ITER; see figure 22.

6. Rotational data

The 3D structures, which appear in JET as I_p and M_{IZ} toroidal asymmetries, usually rotate [10, 13, 14]. Various types of rotation were identified in JET: nearly uniform multi-turn rotations, locked rotations, rotation reversals and others

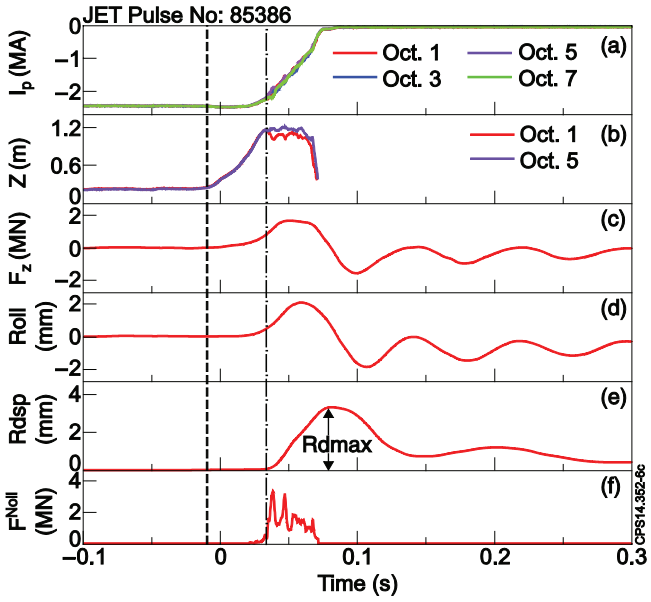

Figure 15. The JET vessel undergoes a complex, damped oscillation: (*a*) plasma currents, (*b*) plasma current centroid vertical displacements, (*c*) vessel vertical (swing) force, (*d*) vessel roll, (*e*) radial vessel displacement, (*f*) sideways force estimation by Noll's formula.

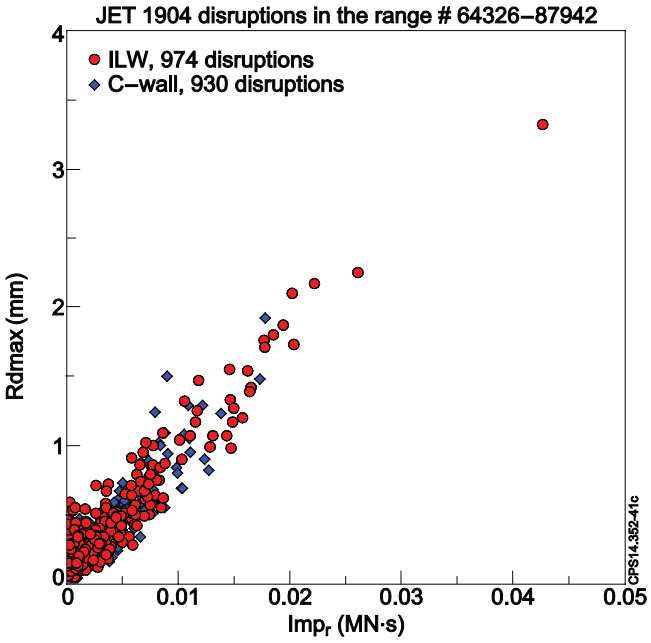

Figure 16. Relationship between directional impulse and JET vessel radial displacement.

[10, 13, 14]. The observed rotation of the I_p asymmetries are in the range of −5 to +10 toroidal turns (a positive value indicates anticlockwise rotation opposite to the negative plasma current and negative toroidal field), where the plasma current and the toroidal field are in the anticlockwise direction, i.e. rotation is most commonly seen in the electron drift direction. The maximum observed numbers of turns are 9.5 (#69311) and 7.9 (#72926) for JET-C and 6.3 (#81990) for JET-ILW. Distributions of the number of rotations for the entire JET-ILW disruption database are shown in figure 23.

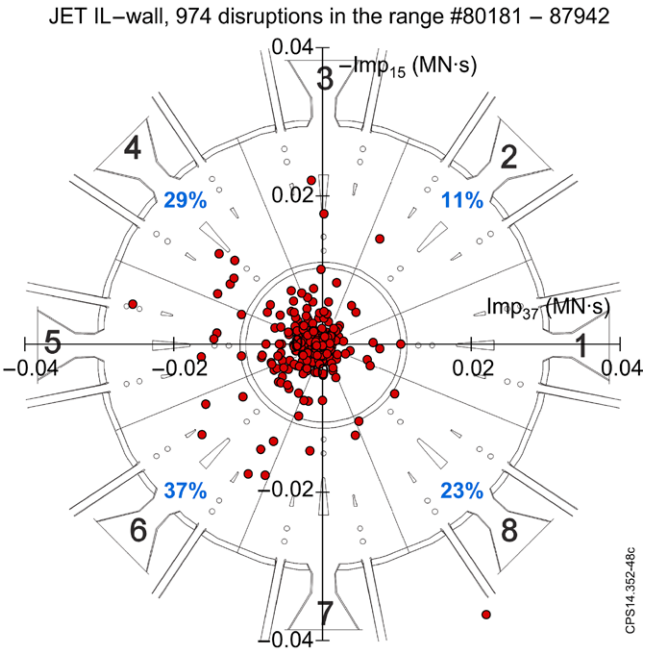

Figure 17. Phase-amplitude distribution of the directional impulses against a JET top vessel view used as background. The percentages show the fraction of the shots which dwell in the corresponding quadrant.

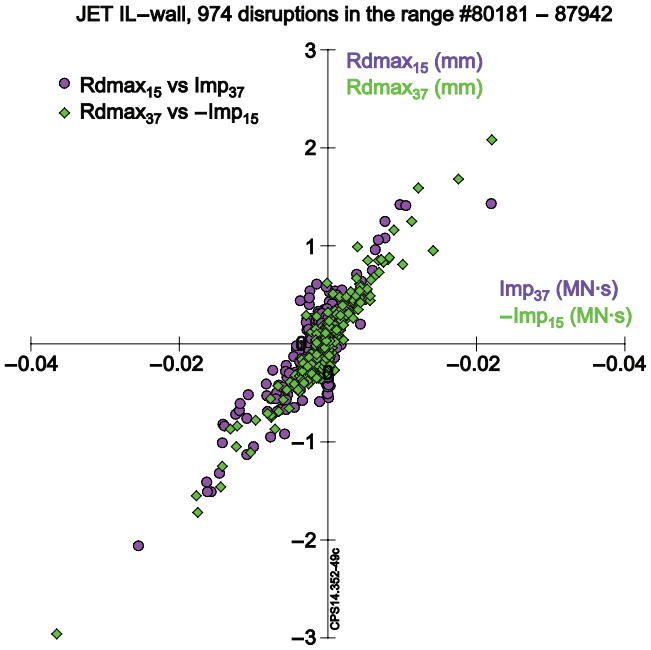

Figure 18. Vessel radial displacement orthogonal components in direction #5 to #1 octants and #7 to #3 octants against the corresponding sideways force impulses.

COMPASS usually reveals nearly locked rotations; see figure 24. However, multi-turn I_p asymmetries rotations were also observed on COMPASS, as shown in figure 7, in contrast to early COMPASS-D data [44].

The uniform multi-turn rotations are of particular concern in large machines because resonance with natural frequencies of the vacuum vessel (and other in-vessel components) could lead to the high dynamic amplification of the forces. There are

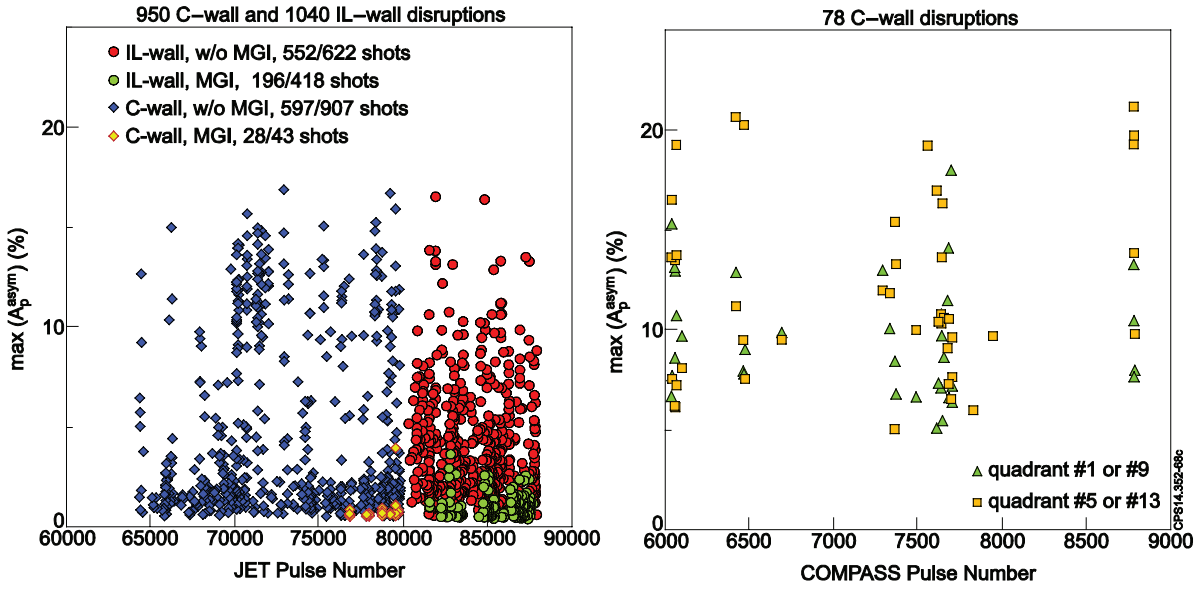

Figure 19. JET and COMPASS amplitude of smoothed I_p asymmetry, where for JET data the first shot number indicates the number in the legend of asymmetrical disruptions and the second number is the total number of recorded disruptions.

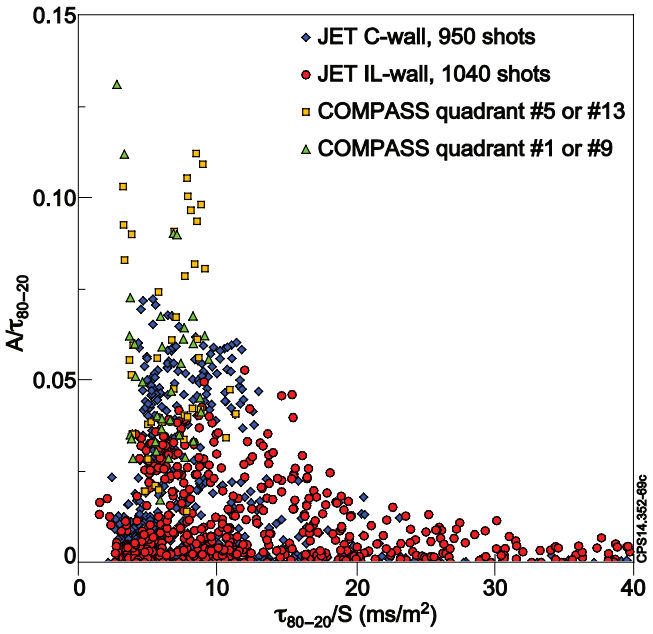

Figure 20. JET and COMPASS data showing the I_p asymmetry integral normalised by the current quench time versus the area normalised CQ time.

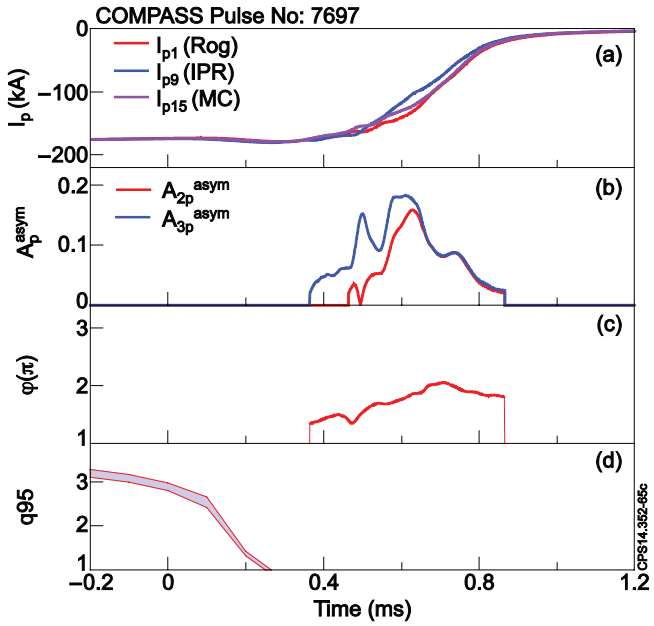

Figure 21. COMPASS extreme asymmetrical disruption: (*a*) plasma currents, (*b*) amplitudes of the I_p asymmetries form I_{p1}, I_{p9}, I_{p15} (A_{3p}^{asym}) and I_{p1}, I_{p9} (A_{2p}^{asym}), (*c*) I_p asymmetry toroidal phase, (*d*) q95 edge safety factor. The time axis is normalised to T_{dis}.

two conditions that must be fulfilled to give dynamic amplification: (a) rotation occurs near a resonance frequency and (b) more than two periods take place [4]. On JET the mechanical resonance period of the vessel (~60–70 ms [45]) is longer than the duration of the rotation (see figure 20, where $S = 3.14$ m^2), hence dynamic amplification is not expected. The ITER mechanical resonance period could be shorter than the duration of rotation leading to the issue of the sideways force dynamic amplification [4]. It is worth mentioning that there is currently no unchallenged understanding or robust model of the rotation behaviour.

7. The edge safety factor at a disruption

The equilibrium reconstruction in JET and COMPASS is performed by using the EFIT code [46]. On JET, the standard ('intershot' in JET jargon) EFIT reconstructions [47] are carried out throughout the disruption until the last converged equilibrium. This allows the trend of the equilibrium parameters from the early stage of CQ to be found. To discriminate between 2D and 3D disruptions, the safety factor time behaviour was checked for the complete JET IL-wall disruption database (1040 disruptions as mentioned in

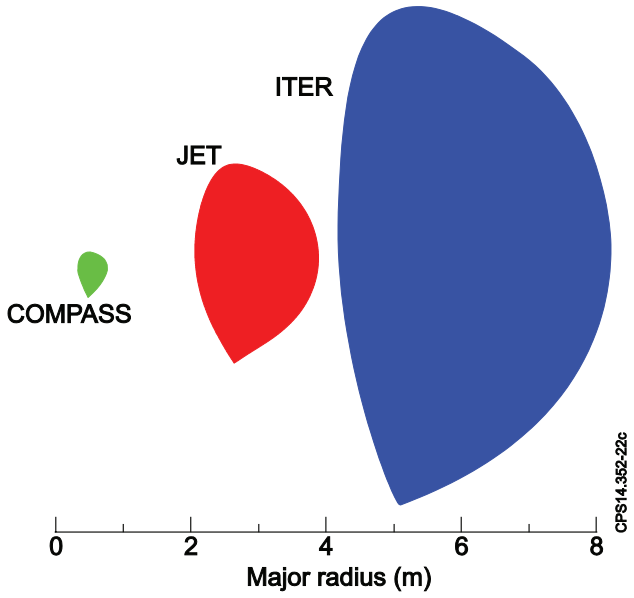

Figure 22. COMPASS, JET and ITER relative dimensions.

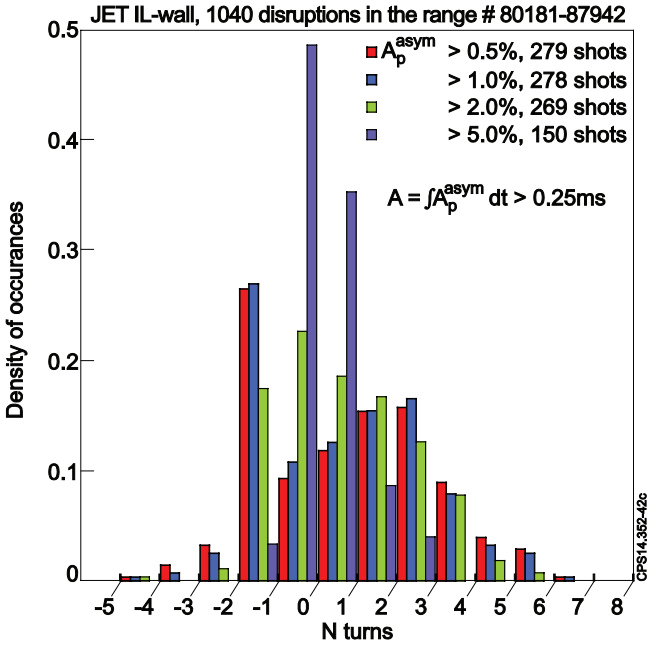

Figure 23. Distributions of the number of rotations for JET-ILW disruptions.

section 3). However, it can be difficult to obtain equilibrium reconstruction in the vicinity of disruptions. Typically, EFIT fails for a few time slices (0.2 ms between slices) among the last two converged equilibria. After a manual analysis of tens of pulses, it was decided to use equilibrium reconstructions if the number of such consecutive faulty slices does not exceed 4.

The most severe (in terms of $A = \int A_p^{asym} dt$) 3D (asymmetrical) disruptions are shown in figure 25. It can be seen in some cases (we term them as a 'first cluster'), which are characterised by large I_p asymmetries and consequently large sideways forces, the development of the toroidal asymmetry precedes the drop to unity of q95. Hence it creates the

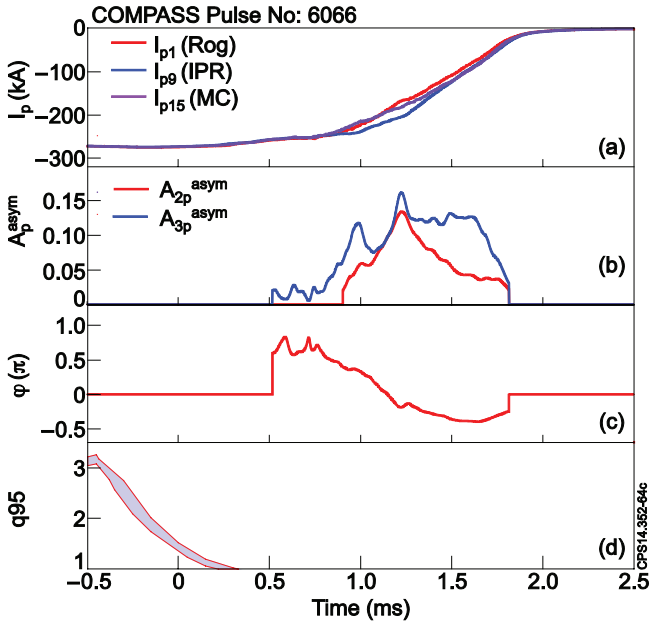

Figure 24. COMPASS I_p asymmetry non-rotational disruption: (*a*) plasma currents, (*b*) I_p asymmetry, (*c*) I_p asymmetry toroidal phase, (*d*) q95 edge safety factor. The time axis is normalised to T_{dis}.

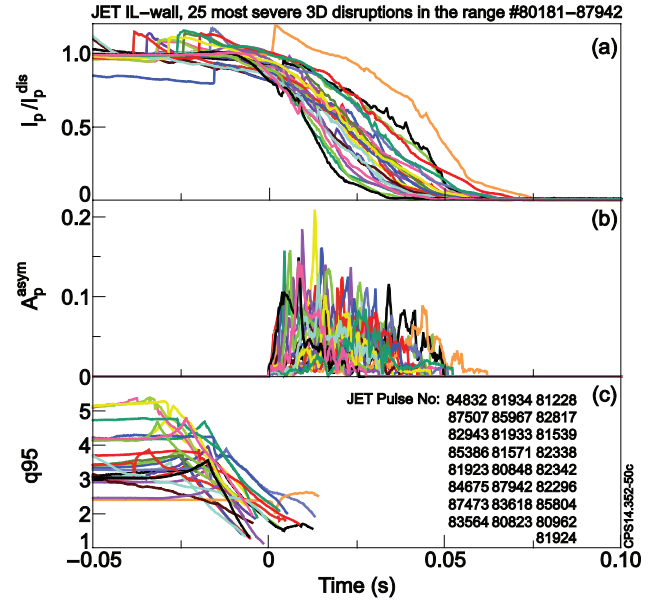

Figure 25. Time traces for the most severe IL-wall asymmetrical (3D) disruptions: (*a*) normalised plasma currents, (*b*) normalised I_p asymmetries, (*c*) safety factor from standard EFIT reconstructions. The time axis is normalised to the I_p asymmetries starting time.

conditions necessary to grow the low *m, n* kink mode. The mode structure analysis was presented in [14] for one specific pulse with a uniformly rotating 3D structure which shows mainly 1/1 kink mode.

There are some non-mitigated disruptions (second cluster), which remain 2D axisymmetric, and in these cases q95 during the early stage of CQ rises from its pre-disruption magnitude; see figure 26. Thus, low *m, n* kink mode magnetohydrodynamic (MHD) stability is not expected to degrade and the I_p asymmetries and the sideways forces remain below the noise level of the magnetic diagnostics.

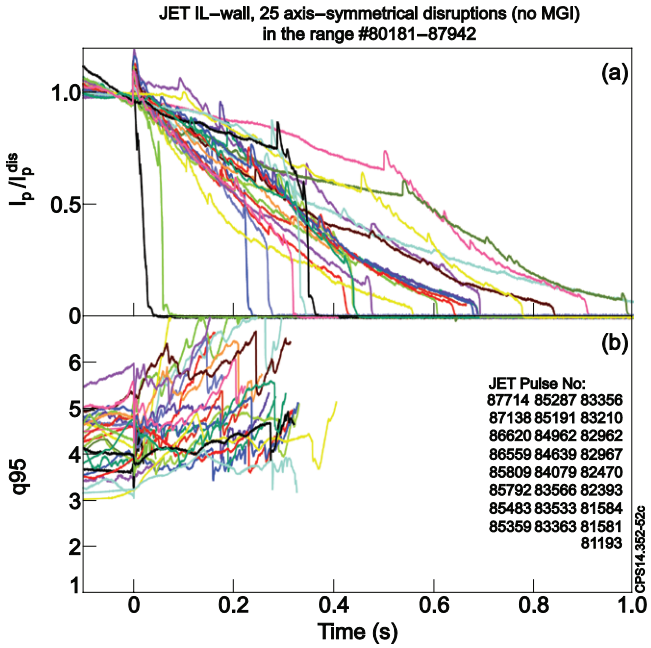

Figure 26. Time traces for IL-wall axisymmetric (2D) disruptions without MGI: (*a*) normalised plasma currents, (*b*) safety factor from standard EFIT reconstructions. The time axis is normalised to T_{dis}.

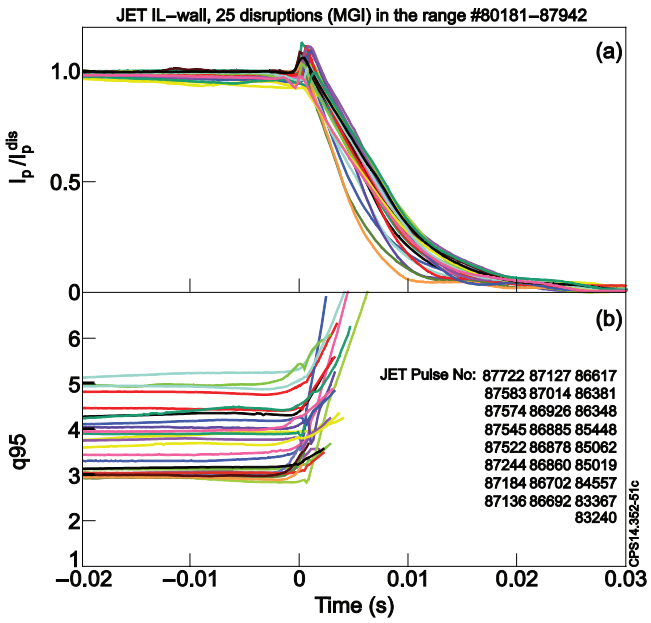

Figure 27. Time traces for IL-wall axisymmetric (2D) disruptions with MGI: (*a*) normalised plasma currents, (*b*) safety factor from standard EFIT reconstructions. The time axis is normalised to T_{dis}.

In MGI-mitigated disruptions (third cluster) q95 rises significantly and any 3D features are below the magnetic diagnostic noise level; see figure 27. q95 growth makes development of the low *m, n* kink mode impossible. The third cluster of disruptions is axisymmetric and 2D.

The effect of the safety factor magnitude on the severity of the I_p asymmetry for the whole IL-wall disruption database is summarised in figure 28. The points represent the last 'reliable' (see above, section 7) converged equilibrium from standard EFIT reconstructions. The severest I_p asymmetry occurs when the edge safety factor approaches q95 = 1.

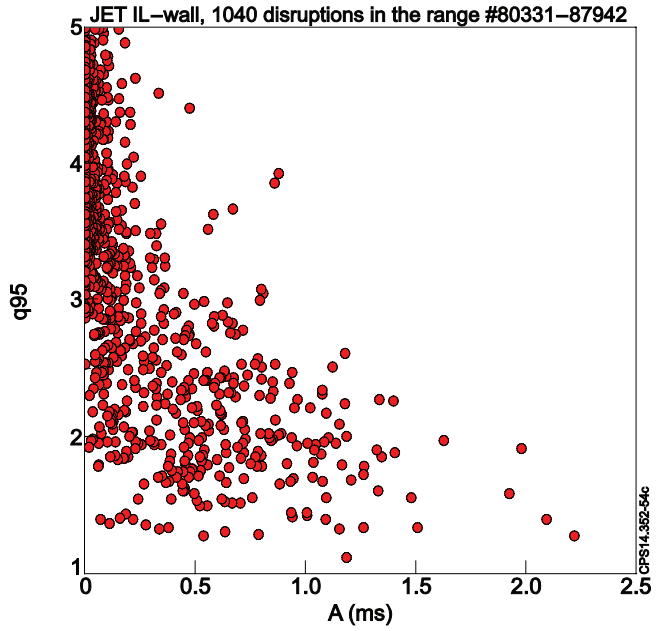

Figure 28. Safety factor from standard EFIT reconstructions. The points represent the last 'reliable' (see definition in section 7) converged equilibrium.

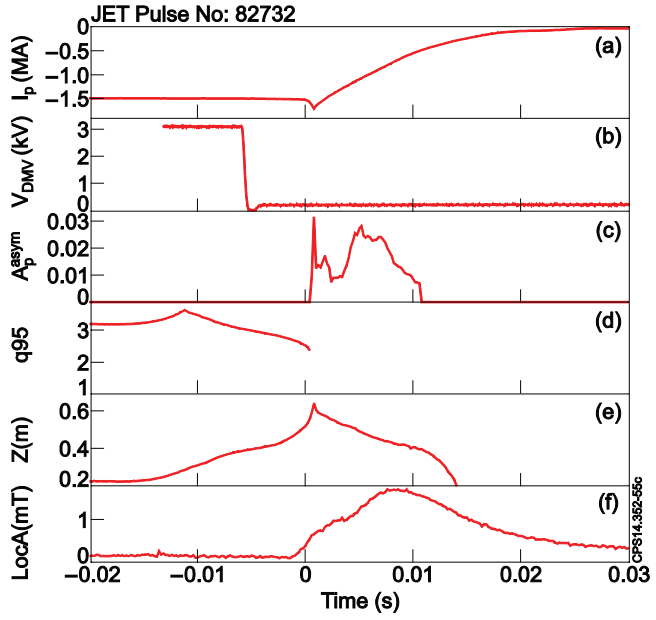

Figure 29. An example where MGI was not 100% efficient as it fired in developed VDE. (*a*) Toroidally average plasma currents, (*b*) DMV voltage drop indicates the activation time, (*c*) I_p asymmetry, (*d*) safety factor from standard EFIT reconstructions, (*e*) vertical current centroid displacement, (*f*) locked mode amplitude. The time axis is normalised to T_{dis}.

There are some disruptions in which MGI with proper pressure and gas composition was not 100% efficient. Figure 29 presents a disruption when MGI fired into a developed VDE. Here the MGI does not prevent a decrease of q95 with time. Hence, the I_p asymmetry occurs at a relatively small value. The locked mode appears directly before the disruption and it is immediately followed by I_p asymmetry. It may be suggested that the locked mode was converted to I_p asymmetry for this specific disruption.

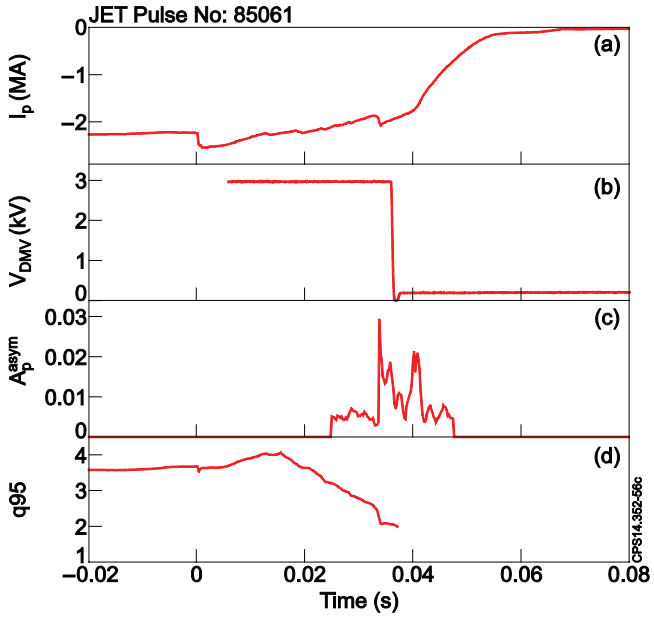

Figure 30. A case where MGI was not 100% efficient as it fired too late. (*a*) Toroidally average plasma current, (*b*) DMV voltage drop indicates the activation time, (*c*) I_p asymmetry, (*d*) safety factor from standard EFIT reconstructions. The time axis is normalised to T_{dis}.

Sometimes the MGI was fired too late, but still reduced the level of the I_p asymmetry somewhat; see figure 30. Such cases should be treated as an MGI fault.

On COMPASS, the standard EFIT [48] reconstruction uses a basic set of inputs: toroidal field, plasma current, currents in PF coils and 16 tangential pick-up coil measurements. The q95 data presented were calculated in manual EFIT runs for a time resolution of 0.1 ms and were cross-checked against runs with different EFIT settings (different weights of individual inputs, different convergence criteria and higher degree of polynomial of current profile representation). The EFIT-induced current module was used to calculate toroidally symmetrical eddy currents in the vacuum vessel with fixed location of an elliptical plasma current cross-section [48]. The reconstructions with various EFIT setups exhibit a small variation ($\leqslant$15%) of q95. The COMPASS examples of the q95 behaviour are shown in figures 7, 21 and 24.

The whole of the IL-wall JET disruption database and the limited number of COMPASS disruptions examined confirm that the development of the toroidal asymmetry precedes the drop of q95—sometimes down to unity.

8. Asymmetry in the toroidal magnetic flux and its possible physical interpretation

In addition to toroidal asymmetry of the plasma current, the toroidal asymmetries are clearly visible as an asymmetry in the in-vessel poloidal voltage (i.e. the toroidal magnetic flux or diamagnetic signal derivatives) measured at 5 kHz in JET since 1994.

Two characteristic cases can be distinguished in the data: the ‘rotational’ mode and the ‘locked’ one, as shown in figure 31. There is clear phase correlation between the asymmetry of plasma currents, vertical plasma current centroid displacements and poloidal voltages for a uniform rotational mode, as shown in figure 31(i), where the associated time window is marked by blue and green.

As explained in [22, 25], the toroidal asymmetry in the plasma currents is related to the MHD effect of the magnetic flux conservation, which generates the negative currents (that we termed Hiro currents) in the wall at the wetting zone of the plasma contact with the plasma-facing wall structures. Understanding of the asymmetry in the diamagnetic signal requires a step beyond the MHD model.

Let us first consider a simple case of an axisymmetric vertical disruption. The additional physics of VDE are illustrated by figure 32 (generated by the VDE code recently developed in PPPL). In simulations, the vertical motion of initially unstable elongated plasma is stopped by the excitation of the toroidal Hiro currents along the tile covered surface, which is consistent with the recent measurements on the EAST device [49]. The eddy currents in the wall contribute to the force balance as well. The plasma shape at the wetting zone becomes conformal to the tile surface with two Y-points in the PF structure at the edges of the Hiro current layer.

The later plasma evolution and shrinking of its cross-section is controlled by the decay of the Hiro currents. At this stage of the VDE the plasma core shrinks and releases its particles to the open field line, thus creating and maintaining the halo zone. The loop voltage due to the presence of the negative Hiro currents and shrinkage of the plasma cross-section drives the force-free compensation current (to compensate for both toroidal Hiro current and of the shrinkage of the cross-section) at the edge of the plasma core. The loop voltage also drives the halo current, which is charged plasma particles driven to the wall along the open field lines in the halo zone. These halo currents are limited by the particle source and, unlike Hiro and eddy currents in the wall, play a minor role in the global force balance. In order to emphasise these two properties, they are referred to here as Evans currents (introduced in [25]), which distinguishes this type of halo current from its conventional concept [50], which assumes an association with the large forces.

The particles released from the plasma core determine the ‘source-limited’ Evans currents in the halo zone I^{Ev} as

$$I^{Ev} \leqslant e\frac{dN_e}{dt}, \tag{14}$$

where e is the electron charge and N_e is the number of electrons in the plasma core.

Note that the poloidal component of the Evans currents creates an extra paramagnetic toroidal flux in the halo zone, which can be measured by diamagnetic loops.

For the 3D case of the VDE, with a developed kink mode, the simulations that would give the geometry of the plasma cross-section, wetting zone and magnetic field are not yet possible. An illustration of such an asymmetrical VDE in JET is presented in figure 33. The halo zone is expected to be wide at the Hiro current area of the plasma contact with the wall where the open field lines are formed. Accordingly, while

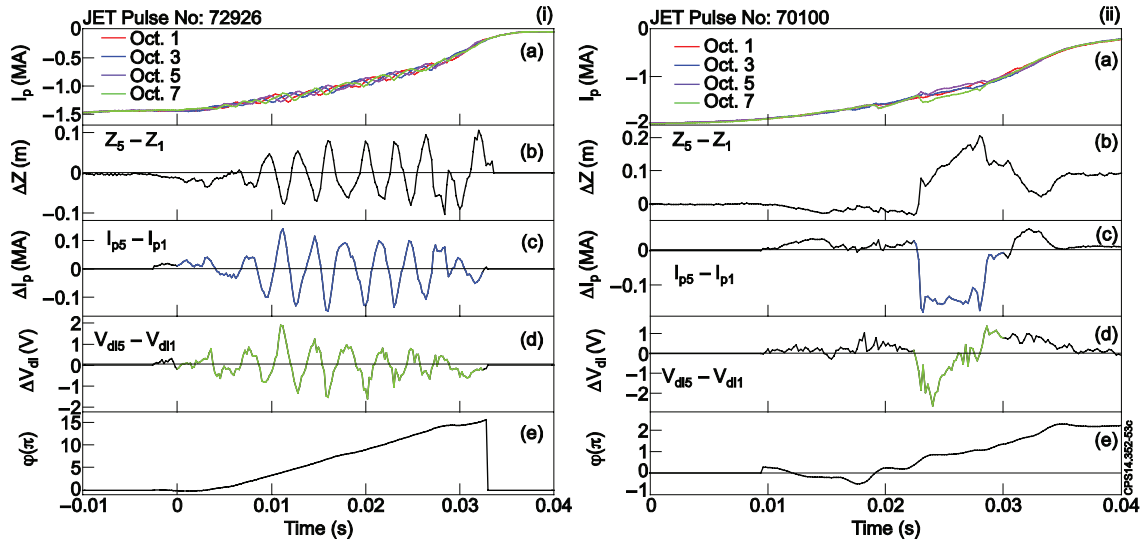

Figure 31. JET I_p asymmetrical disruptions. (i) Rotational mode disruption and (ii) 'locked' mode disruption: (*a*) plasma currents, (*b*) asymmetry of the vertical current centroid displacement, (*c*) I_p asymmetry, (*d*) V_p poloidal voltage asymmetry, (*e*) I_p asymmetry toroidal phase. The time axis is normalised to T_{dis}.

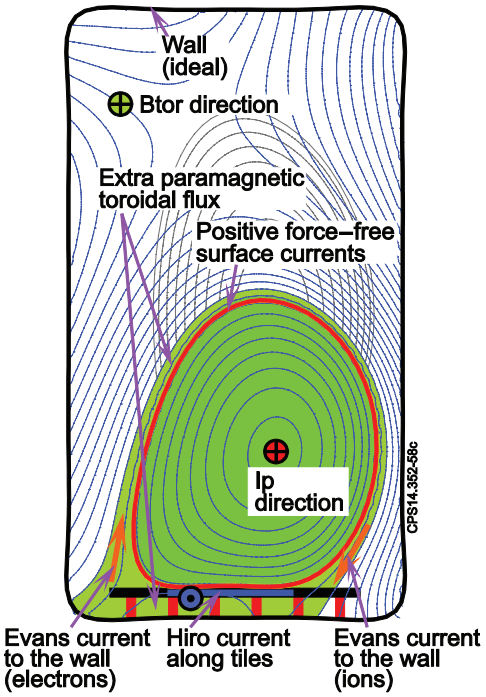

Figure 32. Simulation by VDE code. Illustrative example of an initially unstable (grey shadowed flux surfaces) plasma cross-section and intermediate equilibrium configuration maintained by the toroidal Hiro along the tile surface with the plasma core and the halo zone with the Evans currents.

the toroidal flux inside the plasma core is the same in all its poloidal cross-sections, the Evans currents in the wider halo zone near the plasma contact generate the extra paramagnetic flux at the wetting zone.

The sign of the asymmetry on the diamagnetic voltage in figure 31(i) is consistent with this explanation. Based on the total particle charge inventory in the JET plasma shots #72926 and #70100 of $Q \simeq 600$–700 C and the $t_{cq} \simeq 30$ ms CQ time, the source limitation on the Evans current would be expected to be $Q/t_{cq} \sim 20$ kA. The necessary level of the Evans currents to explain the toroidal flux asymmetry can be assessed from the general expression $\Phi = BS$ (where Φ, B and S are the magnetic flux, magnetic field and area, respectively) as

$$I^{Ev} \cong \frac{1}{\mu_o} \int^t \Delta V_{dl} dt \cdot \frac{L^{Ev}}{S^{halo}}, \qquad (15)$$

where μ_o is the vacuum magnetic permeability, L^{Ev} is the toroidal length of the Evans current circuit and S^{halo} is the cross-section area of the halo zone. The time integral gives the excess of the toroidal flux in the halo zone. Using $L^{Ev} = 5$ m and $S^{halo} = 0.2$ m^2 as the reference numbers, then $\Phi = \int^t \Delta V_{dl} dt \simeq 1.0$ mWb (#72926), and the estimate for the rotational kink mode gives $I^{Ev} \simeq 20$ kA, which is consistent with the limit estimates. For the locked mode (#70100) $\Phi \simeq 2.0$ mWb the similar estimate is $I^{Ev} \simeq 40$ kA, which exceeds the source limitations and explains the decay of the diamagnetic voltage in the locked kink mode case seen in figure 33 due to the saturation of the Evans currents.

It is worth noting that the toroidal flux inside the plasma core is the same in all poloidal cross-sections of 3D equilibrium, hence the 3D effect alone cannot explain toroidal variations of the measured toroidal flux without some wall touch involvement.

9. Unfavourable effect of the MGI disruption mitigation

MGI is routinely used to mitigate disruptions in JET. In 2014 (from #86025 shot onward), MGI was successfully fired into 66% of the disruptive shots. As described above, MGI prevents large sideways forces leading to a greater degree of axisymmetry. However, MGI also produces fast plasma CQ and respectively high vessel eddy currents, as shown in figure 34, where the amplitude of the eddy current in the JET passive

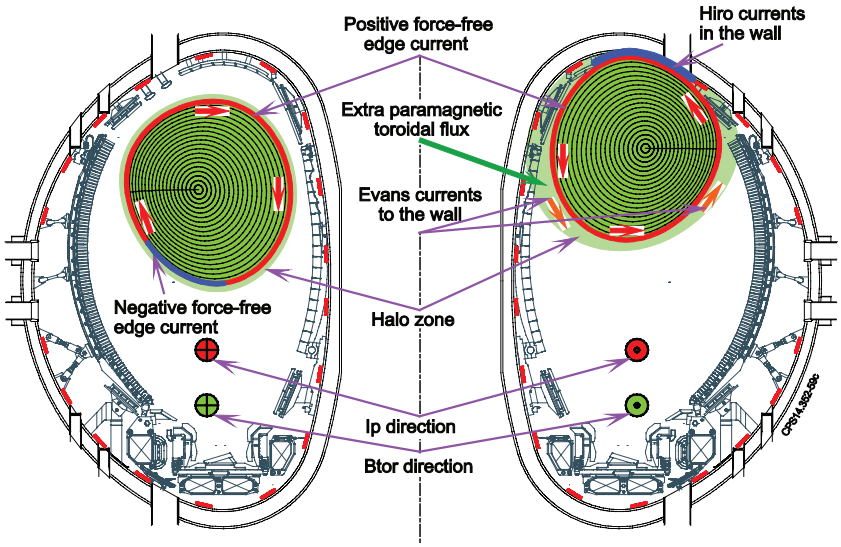

Figure 33. Interpretation of the observed toroidal magnetic flux asymmetry during a VDE with a kink mode. A wide halo zone in the vicinity of the plasma-wall contact shown with the Hiro and Evans currents. The Evans currents generates the extra paramagnetic flux in the wetting zone.

structure is shown, as defined by (3) for the C- and IL-wall, for MGI and non-MGI disruptions.

The MGI disruption $\tau_{80\text{-}20}$ CQ times are mainly in the 10–20 ms region with the normalised amplitude of the eddy current up to 30%; see figure 35.

Electromagnetic simulations of the eddy currents induced in the JET vessel were done with the 3D EM code CARIDDI [51]. The model includes the vessel, the restraint rings and divertor structures. The currents induced in these structures are correctly taken into account in the overall computation. The iron core is also included in the model with its 3D geometry. An axisymmetric disruption has been considered, in which the plasma CQ has been simulated as fixed toroidal filaments carrying a linearly time-varying current. The computation was done for several different linear CQ times. The currents in the PF coils have been assumed as constant during the event, although the real PF currents vary in time due to inductive couplings and voltages imposed by the power supplies. However, even with this approximation, there is some agreement between the modelling results and the experimental data, as can be seen in figure 35.

The peak eddy current density distribution for 1 MA plasma with a 20 ms linear time-varying CQ is shown in figure 36. The induced current tends to bypass the ports flowing through the extensions. The current density appears higher in regions where the section is smaller—a high current density does not necessarily mean a high current. The model also includes the restraint rings and divertor structures, although they are not shown in the figures for the sake of clarity. The highest eddy current density appears near the ports.

Sometimes disruption can cause damage to in-vessel diagnostics. Figure 37 demonstrates a clearly visible pick-up poloidal coil fault during a special MGI-mitigated disruption. The disruption mitigation valve DMV1 (see figure 10) fired a mixture of 60% (D_2) + 40% (Ar) at 33 bar pressure at 7.5 ms before the disruption ($t = 0$ in figure 37). The maximum

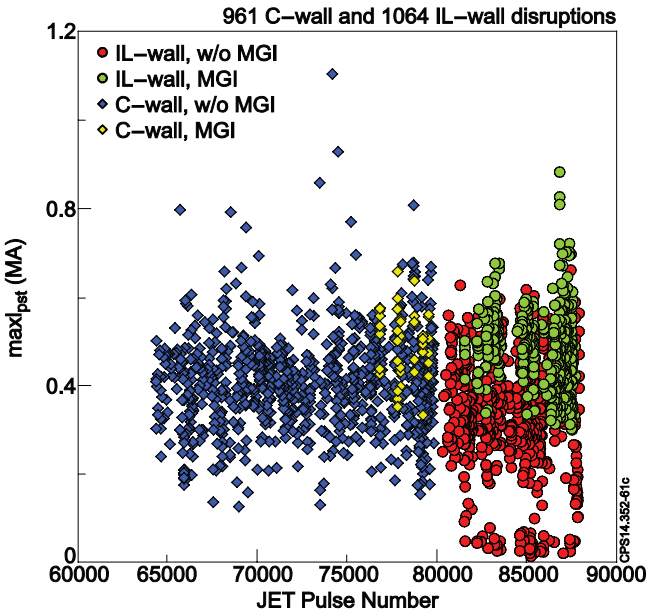

Figure 34. The amplitude of the eddy current induced in JET passive structures; see formula (3) and figure 4.

voltage induced on a similar coil with similar poloidal and toroidal location is ~10 V, occurring at $t = 0$. The maximum eddy current of ~1 MA can be seen at $t = 10$ ms. The pick-up coil (named P803B) failed in between these two events at $t = 5$ ms. It is unlikely that a short ~10 V impulse alone can cause any coil damage. The forces due to the eddy currents cannot affect the coil wires. We can speculate that (a) the absorption of hydrogen and the formation of titanium hydride are a source of damage to titanium coil wires; hydrogen embrittlement can eventually lead to bursting (spalling) of titanium wires; (b) titanium may burn in nitrogen, which is used for seeding experiments in JET [52]; (c) the gas discharge may glow inside the coil shield and shorts the coil. The post-mortem photo presented in figure 38 suggests that events (a) and (b) occurred.

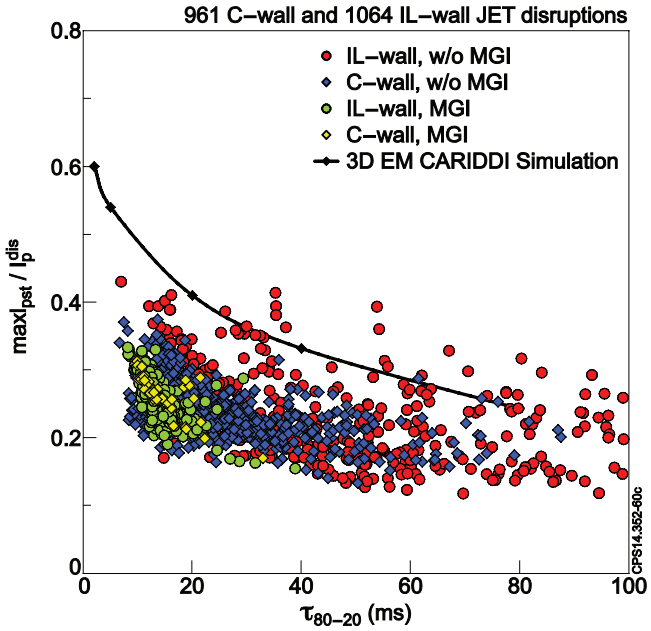

Figure 35. The normalised amplitude of the eddy current induced in JET passive structures, as a function of the CQ time. The black line is the result of the CARIDDI simulation.

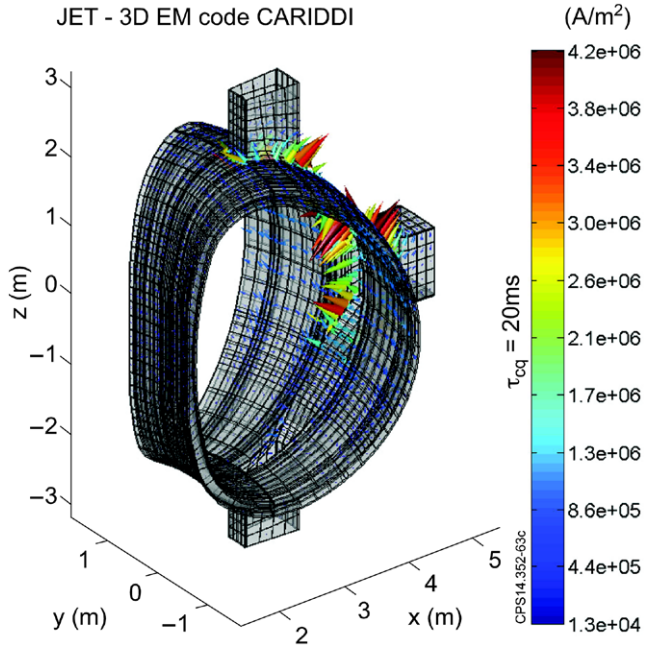

Figure 36. The eddy current density distribution for 1 MA plasma with a 20 ms linear time-varying CQ. The model includes the restraint rings and divertor structures, although they are not shown in the figures for the sake of clarity.

10. Outstanding issues

The sideways force impulses in JET have a preferred toroidal phase that may be caused by intrinsic error fields—this phenomenon requires further investigation.

The MGI is routinely used to mitigate disruptions in JET, but the effect of the resulting large eddy currents and large quantity of gas (particularly hydrogen) used in the injections remains to be assessed.

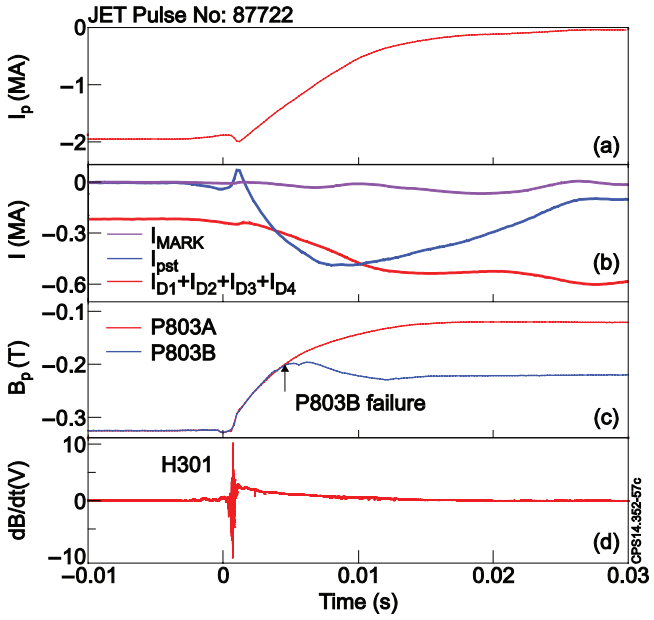

Figure 37. A fault of the poloidal pick-up coil during a special MGI-mitigated disruption; gas: 60% (D_2) + 40% (Ar), pressure: 33 bar, DMV1. (*a*) Plasma current, (*b*) sum of divertor PF currents and eddy currents, (*c*) waveforms of two neighbouring pick-up coils in octant #8, (*d*) d*B*/d*t* H301 coil. The time axis is normalised to $T_{\rm dis}$.

The toroidal asymmetries are clearly visible as toroidal plasma current asymmetries and poloidal voltage (i.e. paramagnetic flux derivative) asymmetries. The physical interpretation provided in section 8 could be improved by taking into account additional observations. The correlation between the toroidal and poloidal vessel current asymmetries provides an opportunity for the calibration of the numerical models.

The simulation with the 3D EM code CARIDDI used the PF circuit with a fixed current, which is not physically accurate. A more self-consistent simulation would be to consider the PF coils with their actual resistance and driving circuit.

Four or more toroidally distributed plasma current measurements on COMPASS will definitely improve the accuracy of the analysis.

11. Summary

The presented data cover the period of JET operations from 2005 until late 2014, and recent COMPASS data. The latter have been found to be in line with the large JET disruption database in terms of amplitude of the plasma current asymmetries and toroidal rotation behaviour.

The observed rotation of the $I_{\rm p}$ asymmetries are in the range of -5 to $+10$ toroidal turns, which cover the domain of the possible dynamic amplification of the sideways forces in ITER.

The IL-wall JET disruption database and all of the examined COMPASS disruptions confirmed that the development of the toroidal asymmetry precedes the drop of q95—sometimes down to unity.

JET radial vessel displacement correlates with sideways force directional impulse, which is estimated only from the magnetic diagnostic. Hence the estimation of the magnitude

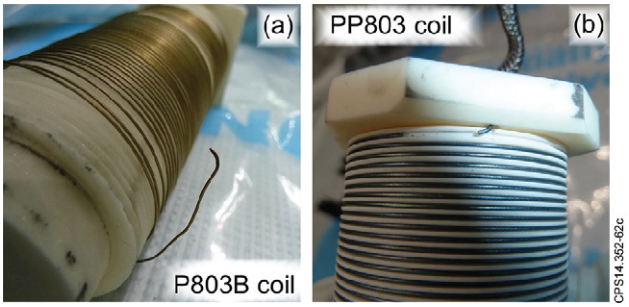

Figure 38. (*a*) P803B faulty poloidal pick-up coil: this post-mortem photo suggests the titanium wire reacted with nitrogen (golden colour); (*b*) another PP803 faulty poloidal pick-up coil located near P803B: this post-mortem photo suggests the titanium wire was contaminated by hydrogen (black colour).

and direction of JET radial vessel displacement can be carried out with only the magnetic measurements.

For the first time the asymmetries in toroidal flux measurements by the diamagnetic loops and their possible physical interpretation is presented.

The JET and COMPASS study on 3D effects during the I_p CQ provides unique experimental data that can help to improve the understanding of disruptions and to develop and to calibrate numerical models, which could be used to predict the loads with future machines, such as ITER.

MGI significantly reduces the I_p asymmetries during the plasma CQ, leading to a greater degree of axisymmetry and thus preventing large sideways forces in JET. However, MGI produces fast CQ and respectively high vessel eddy currents, which expose the machine to additional stresses. The large quantity of gas (particularly hydrogen) used during injection may create additional problems for in-vessel components.

Acknowledgments

This work has been carried out within the framework of the EUROfusion Consortium and has received funding from the Euratom research and training programme 2014–2018 under grant agreement no. 633053 and from the RCUK Energy Programme (grant no. EP/I501045). To obtain further information on the data and models underlying this paper please contact PublicationsManager@ccfe.ac.uk. The views and opinions expressed herein do not necessarily reflect those of the European Commission. This work was also part-funded by the CR Ministry of Education, Youth and Sports grant #LM2011021, by US DoE contract no. DE-AC02-09-CH11466, by Italian MIUR under PRIN grant 2010SPS9B3 and by the Chinese National Magnetic Confinement Fusion Science Program 2011GB105003. The authors would like to acknowledge that some of the data presented were obtained during the IAEA's Joint Experiments on the COMPASS tokamak in 2013 that were organised within the framework of the Coordinated Research Project F13014 on 'Utilization of the Network of Small Magnetic Confinement Fusion Devices for Mainstream Fusion Research'. The authors are grateful to R. Albanese, R. Lobel and V. Riccardo for fruitful discussions during the course of this work, and to S. Newton and N. Gerasimov for proof reading. Conversations with H. Strauss and A. Boozer provided inspiration for JET and COMPASS data analysis.

References

[1] Noll P. *et al* 1996 Present understanding of electromagnetic behaviour during disruptions at JET *Proc. 19th Symp. on Fusion Technology* (*Lisbon, Portugal, 16–20 September 1996*) www.iop.org/Jet/fulltext/JETP96044.pdf
[2] Sugihara M. *et al* 2007 Disruption scenarios, their mitigation and operation window in ITER *Nucl. Fusion* **47** 337
[3] Bachmann C. *et al* 2011 Specification of asymmetric VDE loads of the ITER tokamak *Fusion Eng. Des.* **86** 1915
[4] Schioler T. *et al* 2011 Dynamic response of the ITER tokamak during asymmetric VDEs *Fusion Eng. Des.* **86** 1963
[5] Rebut P.H. *et al* 2010 First experiments in JET *European Physical Society Conf. on Plasma Physics* (*London, UK, 12–19 September 1984*) p 11 www-naweb.iaea.org/napc/physics/FEC/STIPUB670_VOL1.pdf
[6] Thomas P.R. *et al* 2010 MHD behaviour and discharge optimization in JET *European Physical Society Conf. on Plasma Physics* (*London, UK, 12–19 September 1984*) p 353 www-naweb.iaea.org/napc/physics/FEC/STIPUB670_VOL1.pdf
[7] Litunovsky R. 1995 The observation of phenomena during plasma disruption and the interpretation of the phenomena from the point of view of the toroidal asymmetry of forces *JET Internal Report* (contact no. JQ5:11961)
[8] Riccardo V. *et al* 2000 Forces between plasma, vessel and TF coils during AVDEs at JET *Nucl. Fusion* **40** 1805
[9] Riccardo V. *et al* 2009 Progress in understanding halo current at JET *Nucl. Fusion* **49** 055012
[10] Gerasimov S.N. *et al* 2010 Scaling JET disruption sideways forces to ITER *European Physical Society Conf. on Plasma Physics* (*Dublin, Ireland, 21–25 June 2010*) P4.121 http://ocs.ciemat.es/EPS2010PAP/pdf/P4.121.pdf
[11] Riccardo V. *et al* 2010 JET disruption studies in support of ITER *Plasma Phys. Control. Fusion* **52** 124018
[12] Hender T.C. 2010 JET disruption studies in support of ITER *Proc. 23rd Int. Conf. on Fusion Energy 2010* (*Daejeon, Korea, 11–16 October 2010*) (Vienna: IAEA) www-naweb.iaea.org/napc/physics/FEC/FEC2010/papers/exs_10-3.pdf
[13] Gerasimov S.N. *et al* 2012 The rotation of plasma current asymmetries during disruptions in JET *European Physical Society Conf. on Plasma Physics* (*Stockholm, Sweden, 2–6 July 2012*) P5.074 http://ocs.ciemat.es/epsicpp2012pap/pdf/P5.074.pdf
[14] Gerasimov S.N. *et al* 2014 Plasma current asymmetries during disruptions in JET *Nucl. Fusion* **54** 073009
[15] Gerasimov S.N. *et al* 2014 JET and COMPASS asymmetrical disruptions *Proc. 25th IAEA Int. Conf. on Fusion Energy* (*Saint Petersburg, Russia, 13–18 October 2014*) EX/P5-33
[16] Neyatani Y., Yoshino R. and Ando T. 1995 Effect of halo current and its toroidal asymmetry during disruptions in JT-60U *Fusion Technol.* **28** 1634
[17] Granetz R.S. *et al* 1996 Disruptions and halo currents in Alcator C-Mod *Nucl. Fusion* **36** 545
[18] Evans T.E. *et al* 1997 Measurements of non-axisymmetric halo currents with and without 'killer' pellets during disruptions in the DIII-D tokamak *J. Nucl. Mater.* **241–3** 606
[19] Pautasso G. *et al* 2011 The halo current in ASDEX upgrade *Nucl. Fusion* **51** 043010
[20] Gerhardt S.P. *et al* 2012 Characterization of disruption halo currents in the national spherical torus experiment *Nucl. Fusion* **52** 063005

[21] Gerhardt S.P. *et al* 2013 Dynamics of the disruption halo current toroidal asymmetry in NSTX *Nucl. Fusion* **53** 023005
[22] Zakharov L. 2008 The theory of the kink mode during the vertical plasma disruption events in tokamaks *Phys. Plasmas* **15** 062507
[23] Strauss H.R. *et al* 2010 Wall forces produced during ITER disruptions *Phys. Plasmas* **17** 082505
[24] Zakharov L.E. 2010 Comment on 'Wall forces produced during ITER disruptions' *Phys. Plasmas* **17** 124703
[25] Zakharov L.E., Galkin S.A. and Gerasimov S.N. 2012 Understanding disruptions in tokamaks *Phys. Plasmas* **19** 055703
[26] Fitzpatrick R. 2011 Theory of nonaxisymmetric vertical displacement events in tokamaks *Nucl. Fusion* **51** 053007
[27] Boozer A.H. 2012 Rotation of tokamak halo currents *Phys. Plasmas* **19** 052508
[28] Boozer A.H. 2012 Theory of tokamak disruptions *Phys. Plasmas* **19** 058101
[29] Strauss H. *et al* 2013 Sideways wall force produced during tokamak disruptions *Nucl. Fusion* **53** 073018
[30] Boozer A.H. 2013 Tokamak halo currents *Phys. Plasmas* **20** 082510
[31] Strauss H. *et al* 2014 Tokamak toroidal rotation caused by AVDEs and ELMs *Nucl. Fusion* **54** 043017
[32] Strauss H.R. 2014 Toroidal current asymmetry in tokamak disruptions *Phys. Plasmas* **21** 102509
[33] Matthews G.F. *et al* 2011 JET ITER-like wall—overview and experimental programme *Phys. Scr.* **2011** 014001
[34] Romanelli F. *et al* 2012 Overview of the JET results with the ITER-like wall *Proc. 24th Int. Conf. on Fusion Energy* (*San Diego, CA, 8–13 October 2012*) www-naweb.iaea.org/napc/physics/FEC/FEC2012/papers/197_OV13.pdf
[35] Riccardo V. *et al* 2013 Design, manufacture and initial operation of the beryllium components of the JET ITER-like wall *Fusion Eng. Des.* **88** 585–9
[36] De Vries P.C. *et al* 2012 The impact of the ITER-like wall at JET on disruptions *Plasma Phys. Control. Fusion* **54** 124032
[37] Kruezi U. *et al* 2009 Massive gas injection experiments at JET—performance and characterisation of the disruption mitigation valve *36th EPS Conf. on Plasma Physics* (*Sofia, Bulgaria, 29 June–3 July 2009*) P-2.153 http://epsppd.epfl.ch/Sofia/pdf/P2_153.pdf
[38] Lehnen M. *et al* 2013 Impact and mitigation of disruptions with the ITER-like wall in JET *Nucl. Fusion* **53** 093007
[39] Kruezi U. *et al* 2014 A new disruption mitigation system for DT operation at JET *Proc. 28th Symp. on Fusion Technology* (*San Sebastian, Spain, 29 September–3 October 2014*)
[40] Jachmich S. *et al* 2014 Implementation of a new disruption mitigation system into the control system of JET *Proc. 28th Symp. on Fusion Technology, (San Sebastian, Spain, 29 September–3 October 2014*)
[41] Riccardo V., Walker S.P. and Noll P. 2000 Modelling magnetic forces during asymmetric vertical displacement events in JET *Fusion Eng. Des.* **47** 389–402
[42] Pánek R. *et al* 2006 Reinstallation of the COMPASS-D Tokamak in IPP ASCR *Czech. J. Phys.* **56** B125–37
[43] Weinzettl V. *et al* 2011 Overview of the COMPASS diagnostics *Fusion Eng. Des.* **86** 1227–31
[44] Knight P.J. *et al* 2000 Analysis of vertical displacement events and halo currents in COMPASS-D *Nucl. Fusion* **40** 325
[45] Last J. *et al* 1999 Raising the JET toroidal field to 4 T *JET-R* vol 10 (www.iop.org/Jet/fulltext/JETR99010.pdf)
[46] Lao L.L. *et al* 1985 Reconstruction of current profile parameters and plasma shapes in tokamaks *Nucl. Fusion* **25** 1611
[47] O'Brien D.P. *et al* 1992 Equilibrium analysis of iron core tokamaks using a full domain method *Nucl. Fusion* **32** 1351
[48] Appel L.C. *et al* 2006 A unified approach to equilibrium reconstruction *33rd EPS Conf. on Plasma Physics Europhysics Conf. (Rome, Italy, 19–23 June 2006)* (www.iop.org/Jet/fulltext/EFDC060307.pdf)
[49] Xiong H. *et al* 2015 First measurements of hiro currents in vertical displacement event in Tokamaks *Phys. Plasmas* **22** 060702
[50] Strait E.J. *et al* 1991 Observation of poloidal current flow to the vacuum vessel wall during vertical instabilities in the DIII-D tokamak *Nucl. Fusion* **31** 527–34
[51] Albanese R. and Rubinacci G. 1998 Finite element methods for the solution of 3D eddy curreent problems *Adv. Imaging Electron Phys.* **102** 1–86
[52] Giroud C. *et al* 2013 Impact of nitrogen seeding on confinement and power load control of a high-triangularity JET ELMy H-mode plasma with a metal wall *Nucl. Fusion* **53** 113025
[53] Romanelli F. *et al* 2014 *Proc. 25th IAEA Int. Conf. on Fusion Energy* (*Saint Petersburg, Russia, 13–18 October 2014*)